SMHI

METEOROLOGI NR 157, 2015

# The surface processes of the Rossby Centre regional atmospheric climate model (RCA4)

**Patrick Samuelsson[1], Stefan Gollvik[1], Christer Jansson[1], Marco Kupiainen[1]**
**Ekaterina Kourzeneva[2], Willem Jan van de Berg[3]**

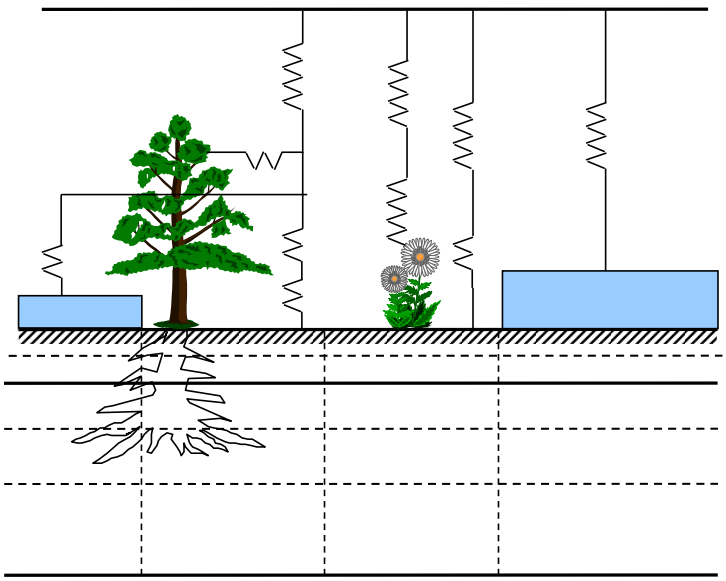

METEOROLOGI Nr 157, 2015

# The surface processes of the Rossby Centre regional atmospheric climate model (RCA4)

**Patrick Samuelsson[1], Stefan Gollvik[1], Christer Jansson[1], Marco Kupiainen[1], Ekaterina Kourzeneva[2], Willem Jan van de Berg[3]**

[1] Swedish Meteorological and Hydrological Institute, (SMHI), Norrköping, Sweden
[2] Finnish Meteorological Institute, (FMI), Helsinki, Finland
[3] Institute for Marine and Atmospheric research Utrecht University, (IMAU), the Netherlands

**Corresponding author**
**Patrick Samuelsson, Swedish Meteorological and Hydrological Institute**
**SE-601 76 Norrköping, Sweden**
**Telephone: +46(0)11 495 8614 E-mail patrick.samuelsson@smhi.se**

**Abstract**

This report describes the physical processes as part of the surface scheme in the Rossby Centre Regional Atmospheric Climate Model (RCA4). Or more strictly for the version used for the CORDEX downscalings with RCA4.

The most important aspects of the surface scheme that are changed with respect to RCA3 are that (i) a new physiography data base is used, (ii) the number of soil layers with respect to soil moisture are increased from two to three and there is also separate soil columns with respect to soil water under forest and open land, respectively, (iii) an exponential root distribution is used, (iv) the density of organic carbon is used to modify soil properties, (v) the prognostic snow albedo is modified to perform better in cold-climate conditions, (vi) Flake is introduced as lake model and lake depth is defined from a global lake-depth data base, (vii) the dynamic vegetation model LPJ-GUESS is introduced for vegetation-climate feedback studies.

# Contents

# 1 Introduction

This report documents the surface schemes of the fourth version of the Rossby Centre Regional Atmospheric Climate Model (RCA4). Or more strictly for the version used for the CORDEX (Coordinated Regional Climate Downscaling Experiment) downscalings with RCA4 (Strandberg et al., 2014).

The land part, the land-surface scheme (LSS), is a tiled scheme with 1–3 main tiles as defined by land-use information and presence of snow; (1) The open land tile is always present, (2) The forest tile is present if land-use includes forest, but limited to maximum 99% area coverage, and (3) The snow tile covers the open land but limited to 99% of the open land part. The open land tile is sub divided into a vegetated and a bare soil part for latent heat flux calculations. The individual fluxes of heat and momentum from these tiles are weighted in order to obtain grid-averaged values at the lowest atmospheric model level according to the fractional areas of the tiles. The forest tile is internally divided into three sub-tiles: forest canopy, forest floor soil, and snow on forest floor. All together this results in 1–5 different surface energy balances depending on if forest and snow are present or not.

The soil is divided into five layers with respect to temperature, with a no-flux boundary condition at three meters depth, and into three layers with respect to soil moisture, with a maximum depth defined by the root depth as given by physiography database. Runoff generated at the bottom of the deep soil layer may be used as input to a routing scheme.

In addition to the soil moisture storages there are six more water storages in the LSS: interception of water on open land vegetation and on forest canopy, snow water equivalent of open land and forest snow, and liquid water content in both snow storages.

The lake model FLake is used for the lake tile of a grid box. The sea tile can be subdivided into a water part and a sea-ice part where a simple two-layer ice scheme is used for prognostic sea-ice variables. Sea-ice fraction is based on boundary data.

Diagnostic variables of temperature and humidity at 2m and wind at 10m are calculated individually for each tile.

For a general description of the role of a LSS in a regional climate model and for documentation of the LSS in RCA3 please refer to Samuelsson et al. (2006). In this report the specific details of Samuelsson et al. (2006) are kept but modified with any updates made. In addition the changes introduced in the surface schemes between RCA3 and RCA4 are documented. These changes concern in general:

- New physiography based on ECOCLIMAP (Section 6.2).
- Number of soil layers with respect to soil moisture are increased from two to three where the thickness of the third layer is defined by the root depth from ECOCLIMAP. There is also separate soil columns with respect to soil water under forest and open land, respectively (Section 2.8.4).
- Exponential root distribution is used with compensation for very dry soil conditions (Section 6.2.1).
- Density of organic carbon is used to modify soil properties with respect to heat conduction, heat capacity and water holding capacity (Section 2.8).
- Prognostic snow albedo is modified to perform better in cold-climate conditions (Appendix B).

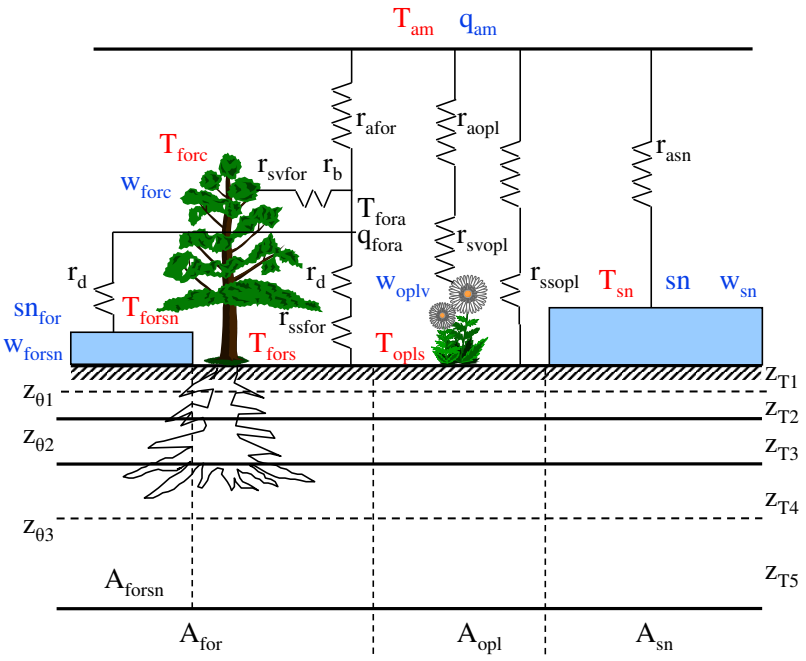


Figure 1: A principal sketch of the land-surface scheme in RCA4. The LSS is divided into three main tiles: forest ($A_{for}$), open land ($A_{opl}$) and snow on open land ($A_{sn}$). The forest also has a snow sub-tile ($A_{forsn}$). Prognostic temperatures are marked in red while the water prognostic variables are marked in blue. Each individual tile is connected to the lowest atmospheric level via their corresponding aerodynamic resistances ($r_a$). For evapotranspiration calculations a number of surfaces resistances are used ($r_s$).

| Parameter | Definition | Reference |
|---|---|---|
| **Sub-grid fractions** | | |
| $A_{for}$ | fractional area of forest | |
| $A_{opl}$ | fractional area of open land | |
| $A_{sn}$ | fractional area of open-land snow | Sec 2.7.1 |
| $A_{forsn}$ | fractional area of snow in forest | Sec 2.7.1 |
| **Prognostic temperatures** | | |
| $T_{opls}$ | open land soil surface temperature | |
| $T_{sn}$ | snow surface temperature | Eq 34 |
| $T_{sns}$ | soil temperature below snow | |
| $T_{forsn}$ | forest snow surface temperature | Eq 26 |
| $T_{fors}$ | forest soil surface temperature | Eq 26 |
| $T_{forsns}$ | soil temperature below forest snow | |
| $T_{forc}$ | forest canopy temperature | Eq 26 |
| **Prognostic water storages** | | |
| $sn$ | open land snow water equivalent | Sec 2.7 |
| $sn_{for}$ | forest snow water equivalent | Sec 2.7 |
| $w_{oplv}$ | intercepted water on low vegetation | Sec 2.2 |
| $w_{forc}$ | intercepted water on forest canopy | Sec 2.2 |
| $w_{sn}$ | snow liquid water | Sec 2.7 |
| $w_{forsn}$ | forest snow liquid water | Sec 2.7 |

| Parameter | Definition | Reference |
|---|---|---|
| **Resistances** | | |
| $r_{svfor}$ | forest canopy surface resistance | Eq 10 |
| $r_{svopl}$ | open land vegetation surface resistance | Eq 10 |
| $r_{ssfor}$ | forest floor soil surface resistance | Eq 17 |
| $r_{ssopl}$ | open land soil surface resistance | Eq 17 |
| $r_{afor}$ | aerodynamic resistance above forest | Sec 2.1 |
| $r_{aopl}$ | aerodynamic resistance above open land | Sec 2.1 |
| $r_{asn}$ | aerodynamic resistance above snow | Sec 2.1 |
| $r_b$ | aerodynamic resistance (forest canopy - canopy air) | Eq 71 |
| $r_d$ | aerodynamic resistance (forest floor - canopy air) | Eq 73 |
| **Depth of soil layers** | | |
| $z_{T1}$–$z_{T5}$ | thickness of soil layers w.r.t. temperature (0.01, 0.062, 0.21, 0.72, 1.89 m) | |
| $z_{\theta 1}$–$z_{\theta 3}$ | thickness of soil layers w.r.t. soil moisture (0.072, 0.21 m, root depth - 0.282) | |

- FLake is introduced as lake model and lake depth is defined from a global lake-depth data base (Section 6.3).
- The dynamic vegetation model LPJ-GUESS is introduced for vegetation-climate feedback studies (Section 5)).

# 2 Land-surface processes

## 2.1 Heat fluxes and aerodynamic resistance

The sensible ($H$) and latent ($E$) heat fluxes between the surface and the first atmospheric level at height $z_{am}$ are parameterized as

$$H = \rho c_p \frac{T_s - T_{am}}{r_a} \tag{1}$$

and

$$E = \rho L_e \frac{q_s(T_s) - q_{am}}{r_a + r_s}. \tag{2}$$

Here, $\rho$ is air density, $c_p$ is heat capacity of the air, $L_e$ is latent heat of vaporisation of water, $T_s$ is surface temperature, $T_{am}$ is temperature at $z_{am}$, $q_s$ is surface saturated specific humidity, $q_{am}$ is specific humidity at $z_{am}$ and $r_a$ aerodynamic resistance. The formulation of the surface resistance $r_s$ depends on the surface as described in Section 2.3.

The aerodynamic resistance is important both for fast response processes such as diurnal temperature range and for long term performance such as a correct division of precipitation into evapotranspiration and runoff. The LSS has three different aerodynamic resistances represented by the characteristics of forest, open land, and snow, with respect to surface temperature and roughness lengths of momentum and heat. The aerodynamic resistance for heat is given by the drag coefficient, $C_h$:

$$C_h = \frac{1}{u_{am} r_a} = \frac{k^2}{\ln(z_{am}/z_{0m}) \ln(z_{am}/z_{0h})} f_h(Ri, z_{am}/z_{0h}), \tag{3}$$

where $u_{am}$ is wind speed at $z_{am}$, $k$ is the von Karman's constant, $z_{0m}$ and $z_{0h}$ are roughness lengths for momentum and heat, respectively, $Ri$ is the Bulk-Richardson number and $f_h$ represents analytic stability functions based on Louis et al. (1981), although modified.

The dependence of the heat fluxes on the aerodynamic resistance is strong. Also, the aerodynamic resistance has been shown to be quite sensitive to the ratio between the roughness length of heat and momentum (Beljaars and Viterbo, 1994; Chen et al., 1997; Samuelsson et al., 2003; van den Hurk and Viterbo, 2003). However, the problem is that estimations of the ratio $z_{0m}/z_{0h}$ vary considerably. According to Chen et al. (1997) it is reasonable to relate the ratio to the properties of the flow as suggested by Zilitinkevich (1995):

$$\frac{z_{0m}}{z_{0h}} = \exp(kC\sqrt{Re^*}), \tag{4}$$

where

$$Re^* = \frac{u_0^* z_{0m}}{\nu}, \tag{5}$$

where $\nu$ is the kinematic molecular viscosity, $Re^*$ is the roughness Reynolds number, and $u_0^*$ is the surface friction velocity. $C$ is an empirical constant which Chen et al. (1997) estimated to be 0.1 based

on comparisons between simulations and observations of heat fluxes. Offline sensitivity studies have shown that $r_a$ is sensitive to the value of $C$ for large values on $z_{0m}$ ($> 0.2$ m) and to the value of $z_{0m}$ for small values on $z_{0m}$ ($< 0.1$ m). Sensitivity studies have also shown that the roughness length provided by ECOCLIMAP can lead to excessively large surface temperatures for open land surfaces. Therefore, the open land roughness length is limited as $z_{0m,opl} = \max(0.05, z_{0m,ECO})$ m for snow free open land, where $z_{0m,ECO}$ represent momentum roughness as given from ECOCLIMAP (Section 6.2). The Zilitinkevich formulation of the ratio $z_{0m}/z_{0h}$ is used for open land and snow surfaces where $z_{0m,snow} = 0.002$ m. For forest we use $z_{0h} = z_{0m}/10$.

## 2.2 Interception of rain on vegetation

Rain intercepted by the vegetation is available for potential evaporation which means that it has a strong influence on the fluxes of heat and consequently also on the surface temperature. Interception of snow by the vegetation is not considered. Below freezing ($T_{forc} \leq 0$°C) rain is intercepted and any water present will stay on the vegetation and evaporate as super-cooled water. The parameterization of interception of rain follows Noilhan and Planton (1989) and its implementation into RCA4 is similar to the implementation in RCA2 as described by Bringfelt et al. (2001). The rate of change of intercepted water is described by

$$\frac{w_{veg}^{\tau+1} - w_{veg}^{\tau}}{\Delta t} = \mathrm{veg}(P - \frac{\delta}{L_e} E_v), \tag{6}$$

where $w_{veg}$ is amount of intercepted water (mm of water on the specified fraction), $\tau$ and $\tau + 1$ represent present and next time step, $\Delta t$ is the length of the time step (s), veg is a vegetation cover parameter provided by ECOCLIMAP (Section 6.2), $P$ is rain intensity (kg m$^{-2}$ s$^{-1}$), $E_v$ is evaporation of intercepted water (W m$^{-2}$), and $\delta$ is the fraction of the vegetation covered with water defined as (Deardorff, 1978)

$$\delta = \left( \frac{w_{veg}}{w_{vegmax}} \right)^{2/3}. \tag{7}$$

The exponent $2/3$ comes from the fact that the intercepted water exists in the form of droplets where the water volume of the droplets is proportional to $r^3$, where $r$ is the radius of the droplets, and the surface of the droplets is proportional to $r^2$. $w_{vegmax} = 0.2 \cdot \mathrm{veg} \cdot \mathrm{LAI}$ is the maximum amount of water allowed on the vegetation (Dickinson, 1984). Here LAI is the leaf area index as defined in Section 2.3.

The evaporation $E_v$ is calculated according to

$$E_v = \rho L_e \frac{q_s(T_s) - q_{am}}{r_a}, \tag{8}$$

i.e. with $r_s = 0$ in Equation 2. To keep the solution numerically stable $\delta$ is solved implicitly

$$\delta = (1 - \alpha) \left( \frac{w_{veg}^{\tau}}{w_{vegmax}} \right)^{2/3} + \alpha \left( \frac{w_{veg}^{\tau+1}}{w_{vegmax}} \right)^{2/3}, \tag{9}$$

where $\alpha$ represents the degree of implicitly (set to 0.5). $w_{veg}^{\tau+1}$ is found by replacing $\delta$ in Equation 6 with Equation 9. The resulting equation is solved using the Newton-Raphson's method.

The new value of intercepted water amount may not exceed the maximum value. Thus, any excess water becomes throughfall, $thr = \max(0.0, (w_{veg}^{\tau+1} - w_{vegmax})/\Delta t)$. The final water amount is corrected with the throughfall as $w_{veg}^{\tau+1} = w_{veg}^{\tau+1} - thr \cdot \Delta t$ and the total amount of rain that falls to the ground becomes $P_{tot} = thr + (1.0 - \text{veg})P$.

This parameterization is used for interception of rain on both forest canopy and on open land vegetation with individual values for the parameters veg and LAI. In the forest case $T_s = T_{forc}$, $q_{am} = q_{fora}$, and $r_a = r_b$ and in the open land case $T_s = T_{opls}$ and $r_a = r_{aopl}$.

For RCA4 ECOCLIMAP provides separate leaf area indexes (LAI) as monthly values for open land vegetation and for coniferous and broadleaved forest, respectively, while for RCA3, due to limited physiography information, LAI was diagnostically calculated as a function of soil temperature (Hagemann et al., 1999) and soil moisture. Thus, for RCA4 the same annual cycle of LAI, interpolated in time between the monthly values, will be used throughout a simulation.

## 2.3 Surface resistances

For latent heat flux a surface resistance is added for vegetation transpiration and for bare soil evaporation. Snow surfaces and intercepted water have zero surface resistance. In the case of condensation, $q_s(T_s) < q_{am}$, the surface resistance is also put to zero.

The vegetation surface resistance, closely following Noilhan and Planton (1989), is a function of a vegetation dependent minimum surface resistance, $r_{svmin}$, the LAI, and five factors representing ($F_1$) the influence of photosynthetically active radiation, ($F_2$) the effect of water stress, ($F_3$) the effect of vapor pressure deficit, ($F_4$) an air temperature dependence, and ($F_5$) a soil temperature dependence:

$$r_{sv} = \frac{r_{svmin}}{\text{LAI}} F_1 F_2^{-1} F_3^{-1} F_4^{-1} F_5^{-1}. \tag{10}$$

The photosynthetically active radiation is assumed to be $0.55 S\downarrow$, where $S\downarrow$ is the incoming shortwave radiation. The factor $F_1$ is defined as

$$F_1 = \frac{1+f}{f + r_{svmin}/r_{svmax}}, \tag{11}$$

with

$$f = 0.55 \frac{S\downarrow}{S_L} \frac{2}{\text{LAI}}, \tag{12}$$

where $r_{svmax}$ is a maximum surface resistance set to 5000 s m$^{-1}$ and $S_L$ is a limit value of 30 W m$^{-2}$ for a forest and of 100 W m$^{-2}$ for open land vegetation.

The factor $F_2$ varies between 0 and 1 depending on available soil moisture $\theta$:

$$F_2 = \begin{cases} 1, & \text{if } \theta > \theta_{cr} \\ \dfrac{\theta - \theta_{wi}}{\theta_{cr} - \theta_{wi}}, & \text{if } \theta_{wi} \leq \theta \leq \theta_{cr} \\ 0, & \text{if } \theta < \theta_{wi} \end{cases} \tag{13}$$

where $\theta_{wi}$ is the wilting point, $\theta_{cr} = 0.9\theta_{fc}$ and $\theta_{fc}$ is the field capacity. To account for different soil moisture conditions in different root layers the factor $F_2$ is calculated individually for each soil layer which in combination with the other factors actually gives different $r_{sv}$-values for each soil layer. These $r_{sv}$-values are finally weighted with respect to the depth of each soil layer (see Appendix D.2).

Factor $F_3$ represents the effect of vapor pressure deficit of the atmosphere or, as expressed here, in terms of specific humidity (Jarvis, 1976; Sellers et al., 1986):

$$F_3 = 1 - g(q_s(T_s) - q_{am}), \tag{14}$$

where $g$ is a vegetation-dependent empirical parameter set to 0.04 for forest and to zero for open land vegetation. In the forest case $T_s = T_{forc}$ and $q_{am} = q_{fora}$ and in the open land case $T_s = T_{opls}$.

The air temperature has a strong influence on the transpiration with the most favorable conditions at 25°C. The factor $F_4$ describes the air temperature dependence following Dickinson (1984)

$$F_4 = 1.0 - 0.0016(298.0 - T_{am})^2, \tag{15}$$

where $T_{am} = T_{fora}$ in the forest case.

The vegetation does not become active in spring until the soil temperature in the root zone reaches at least 2 K above the melt temperature $T_{melt} = 273.15K$. Therefore, an additional factor, $F_5 = 1 - f(T)$, is added which varies between 0 and 1 for soil temperatures between $T_1 = T_{melt} + 4$ K and $T_2 = T_{melt} + 2$ K following a sinusoidal function originally intended for parameterization of soil freezing as described in Viterbo et al. (1999):

$$f(T) = \begin{cases} 0, & T > T_1 \\ 0.5\left[1 - \sin\left(\dfrac{\pi(T - 0.5T_1 - 0.5T_2)}{T_1 - T_2}\right)\right], & T_2 \leq T \leq T_1 \\ 1, & T < T_2. \end{cases} \tag{16}$$

As for $F_2$, this gives different $F_5$-values for different soil layers depending on their temperature.

Bare soil evaporation is restricted by the soil surface resistance (van den Hurk et al., 2000):

$$r_{ss} = \frac{r_{ssmin}}{1 - f(T)} \frac{\theta - \theta_{wi}}{\theta_{fc} - \theta_{wi}}, \tag{17}$$

where $r_{ssmin}$ represents a minimum value of the surface resistance ($= 50$ sm$^{-1}$). As described in Section 2.8 there is no solid phase of soil water, therefore, $1 - f(T)$ is used to represent the fraction of liquid soil water to total soil water in the top soil layer with $T_1 = T_{melt} + 1$ K and $T_2 = T_{melt} - 3$ K.

## 2.4 Evapotranspiration

In the case of wet vegetation the total evapotranspiration is the sum of evaporation of intercepted water, $E_v$ in Equation 8, and transpiration via stomata, as expressed through Equation 2. The total evapotranspiration, $E_c$, is defined as

$$E_c = \rho L_e h_v \frac{q_s(T_s) - q_{am}}{r_a + r_{sv}}, \tag{18}$$

where the Halstead coefficient, $h_v$, includes the fraction of the vegetation covered with water, $\delta$,

$$h_v = h_v^{tr} + h_v^{int} = (1 - k\delta) + \frac{r_a + r_{sv}}{r_a} k\delta. \tag{19}$$

The coefficient is subdivided into a transpiration part, $h_v^{tr}$, and into an interception part, $h_v^{int}$. The Halstead coefficient, as defined in Noilhan and Planton (1989), is modified by introducing the factor $k$ to take into account the fact that also saturated vegetation can transpire, i.e. when $\delta = 1$ (Bringfelt et al., 2001). $k = 0$ would represent a situation where the intercepted water forms full spheres just touching the vegetation surface and therefore allow full transpiration from the whole leaf surface. $k = 1$ would represent a situation where a water film covers the vegetation completely and no transpiration is allowed. To adhere the interception model as described above, where the intercepted water exists as droplets, we set the value of $k$ to 0.25. Note that in the case of condensation, i.e. $E_c < 0$, $h_v = (r_a + r_{sv})/r_a$.

## 2.5 Forest processes

The forest canopy is characterized by low heat capacity which means that its temperature responds fast to changes in fluxes. Thus, to realistically simulate diurnal variations in 2m-temperature in a forest dominated landscape this effect must be accounted for. Here it is assumed that 2m-temperature in the forest is represented by the air temperature at 2 m height above the forest floor. The forest canopy acts more or less like a cover above the forest floor, therefore, it is really the temperature and specific humidity conditions in the canopy air space, $T_{fora}$ and $q_{fora}$, that set the conditions for heat fluxes between forest canopy, forest floor, and lowest model level in the forest tile. $T_{fora}$ and $q_{fora}$ are diagnostic variables which have to be solved iteratively as described in Appendix D. The heat fluxes are expressed as:

| | **Sensible heat flux** | **Latent heat flux** |
|---|---|---|
| **Forest canopy** | $H_{forc} = \rho c_p \frac{T_{forc} - T_{fora}}{r_b}$ | $E_{forc} = \rho L_e h_{vfor} \frac{q_s(T_{forc}) - q_{fora}}{r_b + r_{svfor}}$ |
| **Forest floor (soil)** | $H_{fors} = \rho c_p \frac{T_{fors} - T_{fora}}{r_d}$ | $E_{fors} = \rho L_e \frac{q_s(T_{fors}) - q_{fora}}{r_d + r_{ssfor}}$ |
| **Forest floor (snow)** | $H_{forsn} = \rho c_p \frac{T_{forsn} - T_{fora}}{r_d}$ | $E_{forsn} = \rho L_e \frac{q_s(T_{forsn}) - q_{fora}}{r_d}$ |
| **Canopy air - Atmos.** | $H_{for} = \rho c_p \frac{T_{fora} - T_{am}}{r_{afor}}$ | $E_{for} = \rho L_e \frac{q_{fora} - q_{am}}{r_{afor}}$ |

(20)

Here $r_b$ and $r_d$ are the aerodynamic resistances between the forest canopy and the canopy air and between the forest floor and the canopy air, respectively. The Halstead coefficient, $h_{vfor}$, is defined by replacing $r_a$ with $r_b$, $r_{sv}$ with $r_{svfor}$, and $\delta$ with $\delta_{forc}$ in Equation 19, respectively.

The bulk aerodynamic resistance $r_b$ and the aerodynamic resistance $r_d$, defined in Appendix A, are both based on Choudhury and Monteith (1988).

Since each sub surface within the forest tile has its own energy balance the net radiation components must be separated between the forest canopy and the forest floor according to

$$\begin{cases} Rn_{forc} = & (1-\chi_{SW})(1-\alpha_{forc})S\downarrow + (1-\chi_{LW})\varepsilon_{forc}(L\downarrow - 2\sigma T_{forc}^4 + L\uparrow_{forfloor}) \\ Rn_{fors} = & \chi_{SW}(1-\alpha_{fors})S\downarrow + \varepsilon_{fors}(L\downarrow_{forfloor} - \sigma T_{fors}^4) \\ Rn_{forsn} = & \chi_{SW}(1-\alpha_{forsn})S\downarrow + \varepsilon_{forsn}(L\downarrow_{forfloor} - \sigma T_{forsn}^4) \end{cases} \tag{21}$$

where $L\downarrow$ is incoming longwave radiation. The longwave radiation components $L\uparrow_{forfloor}$ and $L\downarrow_{forfloor}$ are defined as

$$\begin{cases} L\uparrow_{forfloor} = & \sigma(\varepsilon_{fors}(1-A_{forsn})T_{fors}^4 + \varepsilon_{forsn}A_{forsn}T_{forsn}^4) \\ L\downarrow_{forfloor} = & \chi_{LW}L\downarrow + (1-\chi_{LW})\varepsilon_{forc}\sigma T_{forc}^4 \end{cases} \tag{22}$$

Here $\alpha$ and $\varepsilon$ are albedo and emissivity values, respectively, as specified in Figure 1. In the separation a sky view factor is used describing the degree of canopy closure. It is defined as the fraction of sky that the ground under the canopy sees (Verseghy et al., 1993). As shortwave radiation has a diffuse and direct component the sky view factor is different for short and longwave radiation. The sky view factor for longwave radiation is defined as

$$\chi_{LW} = \exp(-0.5 \cdot \mathrm{LAI}). \tag{23}$$

As an approximation this sky view factor is used to represent also the sky view factor with respect to the diffuse part of the shortwave radiation. The sky view factor for the direct shortwave radiation is defined as

$$\chi_{SWdir} = \exp(-0.5 \cdot \mathrm{LAI}(4 - 3 \cdot scos)), \tag{24}$$

where *scos* represents cosine of solar zenith angle. The sky view factor for shortwave radiation in total becomes a weighted value of the sky view factors for direct and diffuse ($\chi_{LW}$) radiation:

$$\chi_{SW} = (1 - frdiffuse)\chi_{SWdir} + frdiffuse\chi_{LW} \tag{25}$$

The fraction of diffuse radiation, $frdiffuse$, is given from the radiation scheme or from the amount of cloudiness. We apply this sky view factor for both needle-leaf and broadleaf trees.

The total flux at the surface is defined as $\phi_{forx} = Rn_{forx} + H_{forx} + E_{forx}$, where $x$ is one of the sub-surfaces represented by forest canopy, forest soil, or forest snow. The total flux plus heat transfer determine the time evolution of the surface temperatures

$$\begin{cases} \dfrac{\partial T_{forc}}{\partial t} = & \dfrac{1}{C_{forc}}\Phi_{forc} \\ \dfrac{\partial T_{fors}}{\partial t} = & \dfrac{1}{(\rho C)_{fors} z_s}[\Phi_{fors} + \Lambda_s(T_{fors2} - T_{fors})] \\ \dfrac{\partial T_{forsn}}{\partial t} = & \dfrac{1}{(\rho C)_{forsn} z_{forsn}}\left[\Phi_{forsn} + \Lambda_{forsn}(T_{forsns} - T_{forsn})\right] \end{cases} \tag{26}$$

where $(\rho C)_{fors}$ and $(\rho C)_{forsn}$ are volumetric heat capacities and $\Lambda_s$ and $\Lambda_{forsn}$ are heat transfer coefficients as defined in Sections 2.8 and 2.7, respectively. The heat capacity of the forest canopy is defined as $C_{forc} = C_{veg}W_{veg} + C_w\rho_w w_{veg}$, where $C_{veg}$ is the vegetative heat capacity, $W_{veg}$ is the standing mass of the composite canopy, $C_w$ is the specific heat of water, and $w_{veg}$ represents the amount of intercepted water in forest canopy (Verseghy et al., 1993). We assume the same vegetative heat capacity for all types of trees.

## 2.6 Open land and bare soil processes

The open land tile, which includes low vegetation and bare soil, has its separate energy balance represented by the surface temperature $T_{opls}$. The net radiation of the open land tile becomes $Rn_{opls} = (1-\alpha_{opls})S\downarrow + \varepsilon_{opls}(L\downarrow + \sigma T_{opls}^4)$ and the sensible heat flux becomes

$$H_{opls} = \rho c_p \frac{T_{opls} - T_{am}}{r_{aopl}}. \tag{27}$$

The evapotranspiration from low vegetation is parameterized as

$$E_{oplv} = \rho L_e h_{vopl} \frac{q_s(T_{opls}) - q_{am}}{r_{aopl} + r_{svopl}}, \tag{28}$$

where $h_{vopl}$ is defined by replacing $r_a$ with $r_{aopl}$, $r_{sv}$ with $r_{svopl}$, and $\delta$ with $\delta_{oplv}$ in Equation 19, respectively.

The evaporation from bare soil is parameterized as

$$E_{opls} = \rho L_e \frac{q_s(T_{opls}) - q_{am}}{r_{aopl} + r_{ssopl}}. \tag{29}$$

## 2.7 Snow processes

A snow surface is very different from most other surfaces found over land. It is characterized by very high albedo and the snow itself has low heat capacity and very limited heat transfer capability. It is important to realistically simulate the fractional coverage of snow since snow is related to important feedback loops. For example, an overestimated fractional snow cover will lead to an overestimated area averaged albedo. This will reduce the amount of absorbed short wave radiation at the surface and cause a reduction in temperature which will be favourable for further snow accumulation. On the other hand, an underestimation of fractional snow cover during the spring will lead to an underestimated area averaged albedo which will tend to raise the temperature and accelerate the snow melt and a

reduction in snow cover. Unfortunately snow cover is one of the most difficult snow related processes to simulate.

There are two separate snow packs in the present LSS: one on open land, where the fluxes directly communicate with the lowest model layer, and one in the forest, where the fluxes depend on the canopy air temperature and humidity. Except for the albedo, which is prognostic for open-land snow but constant for forest snow, the snow scheme is identical for the two snow packs.

### 2.7.1 Estimation of fractional snow cover

An open-land surface, initially with no snow cover, may be totally snow covered for only a small amount of snowfall. This would imply a very thin snow layer. Since snow has a low heat capacity such a thin layer could cause very rapid temperature changes in a numerical scheme and consequently numerical instability. Thus, for numerical reasons the fractional snow cover must increase gradually with increasing snow amount.

During the growing phase, the snow cover fraction, $A_{sn}$, is parameterized to asymptotically approach a maximum allowed snow cover fraction, $A_{snlim}$ set to 0.985, as a function of the snow water equivalent $sn$ according to

$$A_{sn} = A_{snlim} \tanh(100sn), \tag{30}$$

where the factor 100 is a constant controlling the rate of growth. $A_{snlim}$ is set to less than one for numerical reasons but also because a landscape mostly includes rough surfaces and obstacles that always tend to create snow free areas. For a snow layer not reaching $A_{snlim}$ in coverage the same formulation of snow cover is used during the melting phase.

If the snow pack has accumulated over a long enough time and reached over a certain limit in coverage, set to $A_{snlim} - 0.001$, the snow cover fraction during the melting phase is described differently. According to observations the snow cover for deep snow packs is better correlated with the ratio $sn/sn_{max}$ than with $sn$ itself, where $sn_{max}$ is the maximum snow water equivalent reached during the snow season (Lindström and Gardelin, 1999). To simulate this process we store the memory of the snow pack in $sn_{max}$. When $A_{sn} = A_{snlim} - 0.001$ is reached $sn_{max}$ is set equal to $sn$ and during the rest of the snow season $sn_{max}$ is kept larger than or equal to $sn$. During this period the snow cover fraction is parameterised according to

$$A_{sn} = \frac{sn}{sn_{max}\Delta_{snfrd}}, A_{sn} \leq A_{snlim}, \tag{31}$$

where $\Delta_{snfrd}$ is a snow fraction distribution factor which is estimated to 0.6 based on observations (Lindström and Gardelin, 1999). Thus, during snow melt $A_{sn}$ will be kept at $A_{snlim}$ until $sn = sn_{max}\Delta_{snfrd}$ is reached. The observations indicate that $\Delta_{snfrd}$ is correlated with sub-grid orographic variability. In mountainous areas $\Delta_{snfrd}$ tend to be higher than in less mountainous areas. Based on these observations the following formulation is an option in RCA4

$$\Delta_{snfrd} = 0.6 + 0.001\sigma_{orog}, \Delta_{snfrd} \leq 0.8, \tag{32}$$

where $\sigma_{orog}$ is the degree of subgrid orography calculated as the standard deviation of the orography for a specific grid resolution based on the GTOPO30 database. For the CORDEX simulations however

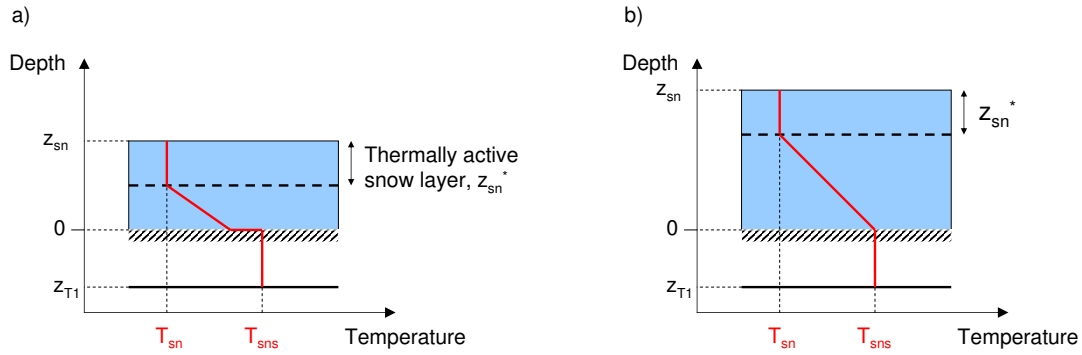


Figure 2: Principal sketch of the assumed temperature profile in a thin (a) and in a thick (b) snow layer respectively.

this option is not applied.

When the end of a snow accumulation period approaches, defined as when $sn^{\tau+1} < k_1 sn^{\tau}_{max}$, $sn_{max}$ is gradually decreased to zero to allow for a new accumulation period to start

$$sn^{\tau+1}_{max} = sn^{\tau}_{max} - (k_1 sn_{max} - sn^{\tau+1})(1-k)/k_1, \tag{33}$$

where $k_1 = 0.2$ and $k = \exp(10^{-6}\Delta t)$.

### 2.7.2 Snow temperature

The purpose of the parameterization of snow in the present LSS is to give a reasonable surface temperature of the snow and a reasonable evolution of the snow pack including runoff of melt water. A correct surface temperature is especially important for the net long wave radiation on the diurnal time scale. On this time scale we assume that only the uppermost part of a thick snow layer is thermally active due to the limited heat transfer capability of snow. Thus, we use a bulk snow layer concept, only regarding the thermal properties of the snow in this layer. There will be a heat transfer also at the snow-soil interface which must be parameterized. Phase changes in the snow between snow and water are important to consider since such processes may have a strong influence on the temperature evolution. To account for these processes any snow melt water is partly kept in the snow as liquid water which can freeze again when the energy balance at the snow surface becomes negative.

Figure 2 shows the concept used describing the assumed temperature profile in the snow for a thin and for a deep snow layer, respectively. The depth of the thermally active snow layer is defined as $z^*_{sn} = \min(z_{sn}, z_{snmax})$, where $z_{sn}$ is the actual snow depth and $z_{snmax} = 0.15$m is the maximum depth of the thermally active snow layer. The actual snow depth is defined as $z_{sn} = sn\rho_w/\rho_{sn}$, where $\rho_{sn}$ and $\rho_w$ are the densities of snow and water, respectively. $\rho_{sn}$ is a prognostic variable in the present LSS as described in Appendix B.

The equation for the prognostic snow temperature is as follows:

$$\frac{\partial T_{sn}}{\partial t} = \frac{1}{(\rho C)_{sn} z_{sn}} \left[\Phi_{sn} + \Lambda_{sn}(T_{sns} - T_{sn})\right], \tag{34}$$

where $(\rho C)_{sn} = (\rho C)_{ice}\rho_{sn}/\rho_{ice}$ is the volumetric heat capacity of the snow and $(\rho C)_{ice}$ is the volumetric heat capacity for ice. $\Phi_{sn} = Rn_{sn} + H_{sn} + E_{sn}$ is the sum of the energy fluxes at the snow surface, net radiation and sensible and latent heat fluxes, respectively, defined as

$$Rn_{sn} = (1-\alpha_{sn})S\downarrow + \varepsilon_{sn}(L\downarrow - \sigma T_{sn}^4), \tag{35}$$

$$H_{sn} = \rho c_p \frac{T_{sn} - T_{am}}{r_{asn}}, \tag{36}$$

$$E_{sn} = \rho L_e \frac{q_s(T_{sn}) - q_{am}}{r_{asn}}. \tag{37}$$

Note that these equations refer to the open land snow and must be replaced by the corresponding forest equations in the case of forest snow. The snow albedo, $\alpha_{sn}$, is defined in Appendix B.

The snow temperature in the layer below the thermally active layer is in principal unknown which means that the heat transfer at the snow-soil interface is parameterised using a heat transfer coefficient $\Lambda_{sn}$ between the snow and the underlying soil layer. Basically it is assumed that the heat transfer at the snow-soil interface decreases with the depth of the snow layer. $\Lambda_{sn}$ is simply a weighted average of the heat transfer coefficients of snow and soil, respectively, defined as

$$\Lambda_{sn}^{-1} = 0.5\,\frac{z_{sn}}{\lambda_{sn}} + 0.5\,\frac{z_{T1}}{\lambda_T}, \tag{38}$$

where $\lambda_{sn} = \lambda_{ice}(\rho_{sn}/\rho_{ice})^{1.88}$ and $\lambda_T$ is defined in Equation 46 and $\lambda_{ice} = 2.2$ W m$^{-1}$ K$^{-1}$.

The prognostic snow temperature equation is part of a heat conduction problem including the prognostic soil temperature equations. The resulting equation system is solved implicitly.

### 2.7.3 Phase changes in snow

Two types of phase changes can take place in the snow pack; for a positive surface energy balance the snow temperature increases until the melting temperature is reached and melting starts, while for a negative surface energy balance any liquid water in the snow can partly refreeze at the same time as the snow temperature drops. One can use different strategies to numerically solve this phase-change problem. We have chosen to divide the time step into two parts which means that upon melting, one part of the time step is used for increasing the temperature and the other part is used to melt snow while keeping the snow temperature at the melting point. Upon freezing, one part of the time step is used to freeze liquid water while keeping the snow temperature constant and the other part is used to decrease the snow temperature.

The total energy per unit time available for the snow is

$$\Phi_{tot} = \Phi_{sn} + \Lambda_{sn}(T_{sns} - T_{sn}). \tag{39}$$

If $\Phi_{tot} > 0$, we estimate the time, $\Delta t_{dtemp}$, it takes to bring $T_{sn}$ to $T_{melt}$ using Equation 34. If $\Delta t_{dtemp} \geq \Delta t$ the melting temperature is not reached and the snow temperature is calculated using Equation 34 with $\Delta t_{dtemp} = \Delta t$. If $\Delta t_{dtemp} < \Delta t$ Equation 34 is used to bring $T_{sn}$ to $T_{melt}$ and then $\Phi_{tot}$ is used

during the rest of the time step, $\Delta t_{dphase} = \Delta t - \Delta t_{dtemp}$, to melt snow while $T_{sn}$ is kept at the melting temperature. The amount of melted snow, or water, becomes

$$sn_{mel} = \frac{\Delta t_{dphase} \Phi_{tot}}{\rho_w L_f}, \tag{40}$$

where $L_f$ is the latent heat of freezing. This amount is used to increase the amount of liquid water kept in the snow, $w_{sn}$, until it reaches a maximum allowed amount, $w_{snsat} = \Delta_{snsat} sn$, where $\Delta_{snsat}$ is set to 10% following Kondo and Yamazaki (1990). Any excess liquid water goes to the soil.

At negative energy balance for the snow, i.e. $\Phi_{tot} < 0$, the snow temperature should drop but if the liquid water content is non-zero we should also freeze some of the water. In contrast to the straight forward melting processes the parameterisation of the freezing process is not as obvious in the case of $w_{sn} > 0$. How much of the liquid water that should be frozen during a certain time does, in principle, depend on where the water is located in the snow layer and how the characteristics of the heat transfer in the snow looks like. With a snow model as simple as the one described here it is impossible to make any physically valid estimation on this amount. Thus, we are let out to some estimation based on assumptions. The assumptions made here are based on the fact that snow melt mainly occurs at the top of the snow layer and that the melt water is located where melting occurs. The larger the amount of melt water in the snow the deeper it penetrates. We estimate a fraction, $\Delta_{freeze}$, of the liquid water amount that is allowed to freeze according to

$$\Delta_{freeze} = \min\left( \frac{sn_{freeze} \rho_{sn}}{\rho_w} \frac{\Delta_{snsat}}{w_{sn}}, 1 \right), \tag{41}$$

where $sn_{freeze}$ is an assumed depth of snow over which freezing is allowed to be active, set to 0.03 m. In other words, the equivalent water amount corresponding to $sn_{freeze}$ is $sn_{freeze}\rho_{sn}/\rho_w$. The corresponding maximum liquid water amount allowed is given by $sn_{freeze}\rho_{sn}/\rho_w \Delta_{snsat}$ which is related to the actual liquid water amount, $w_{sn}$. The value of $sn_{freeze}$ must be estimated by trial and error examining the simulated snow temperature against observations. $\Delta_{freeze}$ is used to calculate the fraction of the time step to be used for freezing of water, $\Delta t_{dphase} = \Delta_{freeze} \Delta t$. During this time the snow temperature is kept constant, while during the rest of the time step, $\Delta t_{dtemp} = \Delta t - \Delta t_{dphase}$, the snow temperature drops following Equation 34. If the available water is less than the corresponding water given by $\Delta t_{dphase}$, the time for freezing of water is reduced.

The change in open-land snow water equivalent is as follows:

$$sn^{\tau+1} = sn^{\tau} + \frac{\Delta t}{\rho_w} \left[ A_{sn}(F + P_{sn-}) + A_{opl}(F + P_{opl-} - F_{opl+}) + A_{sn} \frac{E_{sn}}{L_e} \right] - sn_{mel}, \tag{42}$$

which includes the three phase changes $P_{sn-}$, rain freezing on cold snow, $P_{opl-}$, rain freezing on cold ground and $F_{opl+}$, snow melting on warm ground. $F$ denotes snowfall (kg m$^{-2}$s$^{-1}$). The change in forest snow water equivalent is given by a corresponding equation.

## 2.8 Soil processes

The soil is characterized by its texture and water content. The scheme uses twelve texture classes which are determined using the soil textural triangle (see e.g. Hillel (1980)) and the sand and clay

content of the soil. Sand and clay fraction of the soil are taken from the FAO-UNESCO global soil map (FAO-Unesco (1981)). For each texture class the thermal and hydrological properties are estimated using the following set of parameters: porosity $\theta_{sat}$ ($m^3m^{-3}$), field capacity $\theta_{fc}$ ($m^3m^{-3}$), wilting point $\theta_{wi}$ ($m^3m^{-3}$), saturated soil matrix potential $\psi_{sat}$ (m), saturated hydraulic conductivity $\gamma_{sat}$ (m $s^{-1}$), Clapp-Hornberger $b$ parameter and fraction of quarts $f_q$. Parameter values for each soil texture class are provided in Table 6. In addition to the twelve texture classes representing mineral soils there is an optional organic soil parameterization which is described in Section (2.8.3). This option is by default activated for the RCA4 CORDEX simulations.

### 2.8.1 Soil temperature

The soil heat transfer equation applied for each soil layer can be written as

$$[C_T + \Delta C_{fs}]\frac{\partial T_s}{\partial t} = \frac{\partial}{\partial z}\left(\phi^{t,b} + \lambda_T \frac{\partial T_s}{\partial z}\right). \tag{43}$$

where $C_T$ and $\lambda_T$ are the heat capacity and thermal conductivity for soil at moisture content $\theta$ ($m^3m^{-3}$), respectively. The LSS does not account for the solid phase of soil water which means that e.g. the thermal process related to the latent heat of fusion/freezing is absent. However, this process is important to consider since it acts to delay the soil cooling in autumn and the soil warming in spring. To simulate this effect we apply an adjustment of the soil heat capacity, $\Delta C_{fs}$, as suggested by Viterbo et al. (1999), which increases the total soil heat capacity in the temperature range $T_2 = -3$ to $T_1 = +1$°C:

$$\Delta C_{fs} = -0.5\left[\cos\left(\frac{\pi(T_s - 0.5T_1 - 0.5T_2)}{T_2 - T_1}\right)\right]\frac{\pi}{T_2 - T_1} L_f \theta_{fc} \rho_w. \tag{44}$$

The top boundary condition, $\phi^t$, is represented by the total flux at the surface, $\phi_{fors}$ or $\phi_{opls}$ in the cases of forest soil or open-land soil, respectively, or the heat transfer at the soil/snow interface in the cases of snow covered soil in the forest or at the open land as defined in Section 2.7. At the bottom a zero-flux condition is assumed, i.e. $\phi^b = 0$.

When we have snow partly covering the surface over open land and forest we end up with four separate soil columns with different evolutions of their soil temperature profiles. Each column with its specific top boundary condition. Since the soil is divided into five layers in the vertical with respect to temperature this means that we will have 20 prognostic soil temperatures in this case. When the fractional snow cover changes during a time step the soil temperatures in each column are adjusted accordingly to avoid an artificial change of the total heat content of the soil. In the absence of snow we have maximum two soil columns, one for open land and one for forest. In this case no adjustments of soil temperatures are needed.

### 2.8.2 Soil thermal properties

Thermal conductivity of mineral soils are estimated as a combination of the dry and the saturated thermal conductivities. The method is summarized in Peters-Lidard et al. (1998) and uses a normalised thermal conductivity $K_e$ (Kersten number) to weight the dry and the saturated conductivities:

$$K_e = \begin{cases} 0, & S_r \leq 0.1 \\ logS_r, & S_r > 0.1 \end{cases} \tag{45}$$

where $S_r$ is the degree of saturation. The thermal conductivity of the soil $\lambda_T$ (W m$^{-1}$ K$^{-1}$) is weighted as

$$\lambda_T = \lambda_{sat} K_e + \lambda_{dry}(1 - K_e) \tag{46}$$

where $\lambda_{sat}$ and $\lambda_{dry}$ are the saturated and dry mineral soil thermal conductivities, respectively. The dry thermal conductivity is given by

$$\lambda_{dry} = \frac{0.135\gamma_{dry} + 64.7}{2700 - 0.947\gamma_{dry}} \tag{47}$$

where $\gamma_{dry}$ is the dry mineral soil density estimated using porosity and the density of mineral solids (approximated by 2700 kg m$^{-3}$)

$$\gamma_{dry} = (1 - \theta_{sat})2700. \tag{48}$$

The saturated thermal conductivity is expressed as

$$\lambda_{sat} = \lambda_s^{1-\theta_{sat}} \lambda_{water}^{\theta_{sat}(1-f_{ice})} \lambda_{ice}^{\theta_{sat} f_{ice}} \tag{49}$$

where $\lambda_s$, $\lambda_{water}$ and $\lambda_{ice}$ are the thermal conductivities of mineral solids, water and ice, respectively, and $f_{ice}$ is the fraction of frozen soil water. Thermal conductivity of mineral solids depends on the quarts fraction of the soil $f_q$

$$\lambda_s = \lambda_q^{f_q} \lambda_{not\_q}^{1-f_q} \tag{50}$$

where $\lambda_q$ is the thermal conductivity of quarts and $\lambda_{not\_q}$ the conductivity of non-quarts solids given as $\lambda_{not\_q} = 2.0$ (W m$^{-1}$K) if $f_q > 0.2$ otherwise $\lambda_{not\_q} = 3.0$ (W m$^{-1}$K).

The heat capacity of the soil (J m$^{-3}$ K$^{-1}$) is estimated as

$$C_T = C_{min}(1 - \theta_{sat}) + C_{water}\theta(1 - f_{ice}) + C_{ice}\theta f_{ice} \tag{51}$$

where $\theta$ is the soil water content and $C_{min}$, $C_{water}$ and $C_{ice}$ are the heat capacities of mineral soil solids, water and ice (Table 1).

Table 1: Physical properties used for soil thermal estimations

| $\lambda_q$ W m$^{-1}$ K$^{-1}$ | $\lambda_{water}$ W m$^{-1}$ K$^{-1}$ | $\lambda_{ice}$ W m$^{-1}$ K$^{-1}$ | $C_{min}$ J m$^{-3}$ K$^{-1}$ | $C_{water}$ J m$^{-3}$ K$^{-1}$ | $C_{ice}$ J m$^{-3}$ K$^{-1}$ |
|---|---|---|---|---|---|
| 7.7 | 0.6 | 2.22 | $1.942 \cdot 10^6$ | $4.186 \cdot 10^6$ | $1.883 \cdot 10^6$ |

### 2.8.3 Mineral-organic soil mix

The organic soil parameterization combines the physical properties of an organic soil (Table 2) with the mineral soil properties used in Section (2.8.2). The parameterization is based on a method proposed by Lawrence and Slater (2008) in which thermal and hydrological properties are modified to represent a soil including both mineral and organic matter. The method uses global information on soil carbon density provided by the Global Soil Data Task (2000). The soil carbon density determines an organic soil fraction which is used to weight the mineral and organic properties of the soil.

The organic soil fraction $f_c$ is expressed as

$$f_c = \rho_c / \rho_{c\_max} \tag{52}$$

where $\rho_c$ (kg m$^{-3}$) is the soil carbon density and $\rho_{c\_max}$ (=130 kg m$^{-3}$) the maximum soil carbon density. The soil carbon density is distributed uniformly with depth except for boreal and Arctic regions where the soil carbon density increases towards the surface. These vertical distributions roughly follow the typical soil carbon profiles in Zinke et al. (1986).

The following parameters are scaled using $f_c$:

| | | | |
|---|---|---|---|
| Porosity (m$^3$m$^{-3}$) | $\theta_{sat\_mix}$ | $= (1-f_c)\theta_{sat} + f_c\theta_{sat\_org}$ | |
| Dry thermal conductivity (W m$^{-1}$ K$^{-1}$) | $\lambda_{dry\_mix}$ | $= (1-f_c)\lambda_{dry} + f_c\lambda_{dry\_org}$ | |
| Thermal conductivity of soil solids (W m$^{-1}$ K$^{-1}$) | $\lambda_{s\_mix}$ | $= (1-f_c)\lambda_{s} + f_c\lambda_{s\_org}$ | |
| Heat capacity (J m$^{-3}$ K$^{-1}$ ) | $C_{mix}$ | $= (1-f_c)C_{min} + f_cC_{org}$ | |
| Field capacity (m$^3$m$^{-3}$) | $\theta_{fc\_mix}$ | $= (1-f_c)\theta_{fc} + f_c\theta_{fc\_org}$ | (53) |
| Wilting point (m$^3$m$^{-3}$) | $\theta_{wi\_mix}$ | $= (1-f_c)\theta_{wi} + f_c\theta_{wi\_org}$ | |
| Water potential at saturation (m) | $\psi_{sat\_mix}$ | $= (1-f_c)\psi_{sat} + f_c\psi_{sat\_org}$ | |
| Clapp-Hornberger $b$ parameter | $b_{mix}$ | $= (1-f_c)b + f_cb_{org}$ | |
| Saturated hydraulic conductivity (m s$^{-1}$) | $\gamma_{sat\_mix}$ | $= (1-f_c)\gamma_{sat} + f_c\gamma_{sat\_org}$ | |

Thermal conductivity $\lambda_T$ and heat capacity $C_T$ of the mineral-organic soil mix are estimated similar as for the mineral soil (Equations 46 and 51) by substituting the mineral soil properties with the mixed mineral-organic soil properties

$$\lambda_T = \lambda_{sat\_mix}K_e + \lambda_{dry\_mix}(1-K_e) \tag{54}$$

$$C_T = C_{mix}(1-\theta_{sat\_mix}) + C_{water}\theta(1-f_{ice}) + C_{ice}\theta f_{ice} \tag{55}$$

where $\lambda_{sat\_mix}$ is given by

$$\lambda_{sat\_mix} = \lambda_{s\_mix}^{1-\theta_{sat\_mix}} \lambda_{water}^{\theta_{sat\_mix}(1-f_{ice})} \lambda_{ice}^{\theta_{sat\_mix}f_{ice}}. \tag{56}$$

### 2.8.4 Soil moisture, drainage and runoff

The vertical transport of water in the unsaturated soil is usually expressed using Richards equation (Hillel, 1980)

Table 2: Organic soil properties (Lawrence and Slater, 2008)

| $\theta_{sat\_org}$ $m^3m^{-3}$ | $\lambda_{s\_org}$ $W\,m^{-1}\,K^{-1}$ | $\lambda_{dry\_org}$ $W\,m^{-1}\,K^{-1}$ | $C_{org}$ $J\,m^{-3}\,K^{-1}$ | $\theta_{fc\_org}$ | $\psi_{sat\_org}$ m | $b_{org}$ | $\gamma_{sat\_org}$ $(m\,s^{-1})10^{-6}$ |
|---|---|---|---|---|---|---|---|
| 0.9 | 0.25 | 0.05 | $2.5{\cdot}10^6$ | 0.3 | 0.0103 | 2.7 | 100 |

$$\frac{\partial\theta}{\partial t} = \frac{\partial}{\partial z}\left(\lambda\frac{\partial\theta}{\partial z}\right) - \frac{\partial\gamma}{\partial z} + S(\theta,z), \tag{57}$$

where $\lambda$ is the hydraulic diffusivity ($m^2s^{-1}$), $\gamma$ is the hydraulic conductivity ($ms^{-1}$), and $S(\theta,z)$ is a volumetric source/sink term ($m^3m^{-3}s^{-1}$). The hydraulic diffusivity is parameterized according to McCumber and Pielke (1981)

$$\lambda = \frac{b\gamma_{sat}(-\psi_{sat})}{\theta_{sat}}\left(\frac{\theta}{\theta_{sat}}\right)^{b+2}. \tag{58}$$

The volumetric source/sink term generally includes effects of precipitation, runoff, root extraction, and phase changes of ice to liquid water. However, as described above we do not explicitly include any phase changes of ice to liquid water in the soil but instead we parameterize the effect that soil ice would have had on soil heat capacity and root extraction. The hydraulic conductivity term, $\partial\gamma/\partial z$, in Equation 57 is replaced with a drainage/runoff parameterization as part of the $S(\theta,z)$ term. The final sources and sinks in $S(\theta,z)$ then become; supply of water at the soil surface, $S^w(z_0)$, evaporation/condensation at the soil surface, $S^e(\theta,z_0)$, loss due to root extraction, $S^{re}(\theta,z_d)$, and drainage/runoff, $S^{dr}(\theta,z_d)$, at each soil layer/interface $z_d$. No lateral transport of water exists in the scheme. The supply of water at the soil surface is represented by contributions from rainfall, snow-melt water, and throughfall from vegetation. The evaporation/condensation at the soil surface is represented by two terms; one for the forest floor soil, which is the $E_{fors}$ equation in Equation array 20, and one for the open land soil, Equation 29.

The loss due to root extraction is given by the transpiration parts of Equations 20($E_{forc}$) and 28, i.e. with the transpiration components of the Halstead coefficients, $h^{tr}_{vfor}$ and $h^{tr}_{vopl}$.

The drainage/runoff parameterization is based on the so called $\beta$-formulation as used in the hydrological HBV model (Lindström et al., 1997). The drainage can then be written as a source/sink term

$$S^{dr}(\theta,z_n) = S^{dr}(\theta,z_{n-1})\left(\frac{\theta-\theta_{wi}}{\theta_{fc}-\theta_{wi}}\right)^{\beta}, \tag{59}$$

where the upper boundary condition $S^{dr}(\theta,z_0) = S^w(z_0)$ and the resulting runoff is given by $S^{dr}(\theta,z_2)$. The exponent $\beta$ set to zero would imply a grid square with no water holding capacity at all while a high $\beta$ value indicates such homogeneous conditions that the whole grid square may be regarded as a bucket that overflows when its field capacity is reached. $\beta$ is thus more an index of heterogeneity than of soil property. $\beta$is a tuning parameter and in the present model we use $\beta = 2$, which the same value as is used in the HBV model (Bergström and Graham, 1998).

There are three prognosic layers of soil moisture. The thicknesses of the top and second layers are constant (Figure 1) while the thickness of the third layer is given by the root depth according to

ECOCLIMAP. There are also separate soil water columns under forest and open land, respectively. Thus, in total we have six prognostic soil water variables $\theta$.

See Appendix D.4 for details on soil moisture.

# 3 Sea-surface processes

In uncoupled mode RCA4 depends on forcing data for sea-surface temperature (*SST*) and sea-ice cover (*SIC*), e.g. from ERA-Interim or from a GCM. In coupled mode the ocean model provides *SST*, *SIC*, sea-ice/snow temperature (*SIT*) and sea-ice/snow albedo (Wang et al., 2015). Diagnostic variables over the sea tile of temperature and humidity at 2 m and wind at 10 m are calculated using Monin-Obukhov similarity theory as described in Appendix C.

## 3.1 Fluxes

The momentum flux $\tau$ (N m$^{-2}$) is defined as:

$$\tau = \rho u_*^2 f_m(Ri, z_{am}/z_{0m}) = \rho C_d u_{am}, \tag{60}$$

where $u_*$ is the friction velocity, $C_d$ is the neutral drag coefficient for momentum, $u_{am}$ is the wind speed at lowest atmospheric model level $z_{am}$ (at 30 m) and $f_m$ is a correction factor for atmospheric stability, represented by the Richardson number *Ri*.

The neutral drag coefficient for momentum over sea water and ice is

$$C_d = \frac{k^2}{\ln(z_{am}/z_{0ms,i})^2}, \tag{61}$$

where $k$ is the von Karman's constant ($= 0.4$) and $z_{0ms,i}$ is the roughness length for momentum over sea or ice, respectively.

The roughness length over ice is set constant, $z_{0mi} = 8 \cdot 10^{-4}$ m, emitting any effect of ice ridges and other non-smooth ice formations. The roughness length over sea is defined as a function of wind speed interval:

$$z_{0ms} = (1 - f_U)0.11\frac{\mu}{u_*} + f_U \alpha_c \frac{u_*^2}{g}. \tag{62}$$

Here $f_U = 0$ for $U_{z_{am}} < 3$ ms$^{-1}$ and $f_U = 1$ for $U_{z_{am}} > 5$ ms$^{-1}$ with a smooth non-linear transition in between. $\mu$ is the molecular kinematic viscosity of air ($= 1 \cdot 10^{-5}$), $g$ is acceleration of gravity and $\alpha_c$ is the Charnock constant. In coastal regions (land fraction $\geq 0.01\%$) the roughness length of water is increased by increasing the Charnock constant. Thus, over open sea $\alpha_c = 0.014$ while in coastal areas $\alpha_c = 0.032$ (Rutgersson et al., 2001).

The sensible and latent heat fluxes, $H$ and $E$, (W m$^{-2}$) are defined as:

$$H = \rho c_p \frac{T_s - T_{am}}{r_{ah}} \tag{63}$$

and

$$E = \rho L_e \frac{q_s(T_s) - q_{am}}{r_{aq}}, \tag{64}$$

where $T_s$ is surface temperature ($SST$ for sea water, $SIT$ for sea ice/snow and $LST$ for lake) and $r_{ah}$ and $r_{aq}$ are aerodynamic resistances for heat and moisture, respectively. The aerodynamic resistances are given by the drag coefficients, $C_{h,q}$:

$$C_{h,q} = \frac{1}{ur_{ah,q}} = C_d f_{h,q}, \tag{65}$$

where $f_{h,q}$ are stability correction functions for heat and moisture flux, respectively.

### 3.2 Prognostic ice and snow variables

For uncoupled simulations a simple sea-ice/snow parameterisation is used. The temperature of any sea ice ($SIC > 0$) is simulated by a heat-transfer equation for an ice cover with two layers assuming constant ice thickness. The first layer is 0.07 m and the total thickness is 0.5 m in the Baltic Sea and 1 m for the rest of the ocean. Ice albedo is set to 0.5. The heat flux at the ice-water interface is parameterised as 2 $W^{-2}$ $K^{-1}$, referring to the difference in temperature between sea water and bottom ice layer, where sea-water is assumed to be $-0.3$ °C for the Baltic Sea and $-1.865$ °C for the rest of the ocean. Snow on ice is simulated as over land but with the prognostic snow albedo limited to the range 0.7–0.85.

## 4 Lake processes - FLake

FLake is a two-layer bulk model based on a self-similar representation (assumed shape) of the temperature profile in the mixed layer and in the thermocline (Mironov, 2008; Mironov et al., 2010). The model incorporates (i) a flexible parameterisation of the time evolving temperature profile, (ii) an advanced formulation to compute the mixed-layer depth, including the equation of convective entrainment and a relaxation-type equation for the depth of a wind-mixed layer, (iii) a module to describe the vertical temperature structure of the thermally active layer of bottom sediments and the interaction of the water column with bottom sediments, and (iv) a snow-ice module.

FLake carries a number of ordinary differential equations for the quantities that specify the time evolving temperature profile in lakes. These are the temperature and the thickness of the upper mixed layer, the temperature at the water-bottom sediment interface, the mean temperature of the water column, the shape factor with respect to the temperature profile in the thermocline, the temperature of the upper surface of the ice, and the ice thickness. Optionally, the bottom sediment module can be activated to determine the heat flux at the water-bottom sediment interface. In that case two additional quantities are computed, namely, the depth of the upper layer of bottom sediments penetrated by the thermal wave and the temperature at that depth. If the bottom sediment module is switched off, the heat flux at the water-bottom sediment interface is set to zero. If the snow module is switched on, prognostic equations are carried for the temperature at the snow upper surface and for the snow thickness.

Further information about FLake can be found at http://lakemodel.net.

## 4.1 FLake in RCA

For the version of FLake implemented in RCA4 the snow module has not been thoroughly tested. Therefore the snow module is not activated and the presence of snow is taken into account by modifying the ice albedo and the thermal conductivity of ice.

The mean lake depth is the main parameter to which the model is sensitive. Numerical experiments suggest that the lake depth should be limited to 40 m (perhaps 50 m). That is, an artificial lake bottom should be set at a depth of 40 m where the actual lake depth is larger. The use of such device is justified since FLake is actually not suitable for deep lakes (because of the assumption that the thermocline extends from the bottom of the mixed layer down to the lake bottom). Thus, any lake depth given by the lake-depth data base (Section 6.3) is limited to 40 m in RCA.

In RCA all types of inland water (natural lakes, man-made reservoirs and rivers, from hereon collectively referred to as lakes) are modelled by FLake. If the information is available there is a possibility to distinguish between three different lake categories with respect to depth in each grid box; shallow (0-4 m), medium (4-8 m) and deep lakes ($>$8 m). The fractional area of the lakes and their area-weighted depth for each category are specified by combing the information on the lake depth from the database and the lake fraction information from ECOCLIMAP. When no information on the lake depth is available but the ECOCLIMAP data indicates that lakes are present within a grid box, a default depth of 10 m is used. Any fraction of inland water less than 1% is replaced by land using the existing fraction of open land and forest in the grid box.

The fluxes of momentum and heat over inland water are parameterised as for sea according to Section 3.1. Thus, the default FLake turbulent flux parameterisations are replaced in the RCA implementation.

A more detailed description on how FLake is implemented in RCA and how it is applied can be found in Samuelsson et al. (2010).

# 5 Dynamic vegetation - RCA-GUESS

RCA-GUESS (Smith et al., 2011) refers to the model setup in which RCA is coupled with the dynamic vegetation model LPJ-GUESS. During a RCA-GUESS simulation RCA provides climate variables to LPJ-GUESS and LPJ-GUESS returns updated vegetation fractions and LAI to RCA.

LPJ-GUESS (Lund-Potsdam-Jena General Ecosystem Simulator) is an individual based dynamic vegetation model optimized for regional scale applications (Smith et al., 2001). It shares many processes with the global vegetation model LPJ-DGVM (Sitch et al., 2003). However, instead of the large-area parameterization for vegetation structure and dynamics used in LPJ-DGVM, LPJ-GUESS explicitly simulates growths and competition (for space, light and soil resources) among individual trees and understory vegetation. Trees and understory vegetation are parameterized by plant functional types which are a set of parameter values representing plant characteristics such as morphology, phenology, shade and drought tolerance, fire resistance and bioclimatic limits.

During a coupled simulation RCA provides air temperature, net short wave radiation, soil temperature and soil moisture to LPJ-GUESS. The latter two are optional and the user can chose to let LPJ-GUESS handle soil moisture and/or temperature internally. For the forest tile, air temperature is represented

by the canopy air temperature, the net short wave radiation is represented by the forest canopy part and soil conditions are represented by the average (in the presence of snow) forest soil column. For the open land tile, air temperature is represented by T2m over open land, the net short wave radiation is represented by the open land vegetation part and soil conditions are represented by the average (in the presence of snow) open land column. LPJ-GUESS returns updated LAI, fraction of open land and the coverage of deciduous and conifer forests to the RCA land surface scheme which alters the albedo and the surface and aerodynamic resistances and thereby the partitioning of the surface energy fluxes. Surface and vegetation albedo values are prescribed for coupled simulations, i.e. not read from ECOCLIMAP as during normal RCA simulations. The reason for this is that LPJ-GUESS may create vegetation in a grid box which has no correspondence in the currently observed vegetation represented by ECOCLIMAP and therefore no physiography information is defined. RCA-GUESS has successfully been applied for Europe (Wramneby et al., 2010), Africa (Wu et al., 2013) and the Arctic (Zhang et al., 2014).

An approximate steady state between vegetation and the climate is needed to initialize a RCA-GUESS simulation. This is achieved using a two stage spinup. In the first stage, LPJ-GUESS is ran offline for 360 years using observed climate followed by a 30 year coupled simulation. The change from offline to coupled simulation creates a slow adjustment in the vegetation since observed and modeled climate usually differ. To eliminate this adjustment a second spinup phase is applied. This is done by running LPJ-GUESS offline again but forced with output from the recent coupled simulation. The offline simulations is repeated cyclically over 360 years. After this two stage spinup procedure vegetation structure and composition are in equilibrium with the 30 year average climate of the coupled system conditions. In reality the vegetation is seldom in equilibrium with the climate since the time scale of vegetation changes is in the order of 100 years. This spinup procedure is however considered to give a reasonable good approximation of the initial state of the vegetation. Details on the spinup method can be found in Wramneby et al. (2010) (see also Smith et al. (2011) and Zhang et al. (2014)).

# 6 Physiography

## 6.1 Orography

RCA uses the openly available database Gtopo30 (Survey, 1996) to represent the land topography. Gtopo30 has global resolution of approximately $1.0 \times 1.0$ km. For each grid point the associated grid area (called cell from now on) is given the integrated height using the dataset as piecewise constants. To make sure that we do not integrate any data points twice we use an inside/outside algorithm to determine if a data point is inside the cell or not. If $\vec{x}_i$ is inside cell $j$ we use the midpoint quadrature to integrate the data associated with $\vec{x}_i$

$$orography_j = \frac{g}{N} \sum_{n=1}^{N} gtopo30(\vec{x}_n),$$

where $g$ is the gravitational acceleration (in RCA set to constant, 9.80665 $\mathrm{ms}^{-2}$).

## 6.2 Land-use physiography

The land-use physiography in RCA is based on ECOCLIMAP (Masson et al., 2003). The data and source code is according to "ECOCLIMAP_I_GLOBAL" as indicated on the web-page `http://www.cnrm.meteo.fr/surfex/spip.php?article19`. In addition to the ECOCLIMAP data we utilize information on soil carbon (Section 2.8.3).

For RCA purposes we have modified the ECOCLIMAP source code (code_seul.tar.gz):

- Redefined the specifications of `NTILE=3` in `vegtype_to_patch.f90` (see Table 3)
- Added output of `F_lake` in `ecoclimap_parameters.f90`
- Added reading and processing of soil carbon in `ecoclimap_parameters.f90`

The three tiles are defined as:

Table 3: The three land tiles in RCA

| Tile | Description | ECOCLIMAP IVEGTYPE |
|---|---|---|
| t01 | open land low vegetation | `NVT_(all_no_tree)` |
| t02 | coniferous forest | `NVT_CONI` |
| t03 | broadleaf forest | `NVT_TREE` or `NVT_EVER` |

The available ECOCLIMAP parameters in RCA are listed in Appendix E.

### 6.2.1 Root distribution

The root depths for open land and forest, respectively, are specified using the ECOCLIMAP parameters `droot_t1`, `droot_t2` and `droot_t3`:

$$\begin{aligned} D_{root\_opl} &= \max(droot\_t1, 0.332), \\ D_{root\_for} &= \max(droot\_t2, droot_t3, 1.5). \end{aligned} \tag{66}$$

The vertical distribution of roots is parameterised following Jackson et al. (1996). The extinction coefficient $\beta_{root}$ represents how the roots are distributed. High $\beta_{root}$-values correspond to a greater proportion of roots at larger depths. We calculate $\beta_{root}$ assuming that 99% ($Fr_{root} = 0.99$) of the roots occupy the root depth $D_{root}$:

$$\beta_{root} = (1 - Fr_{root})^{\frac{1}{D_{root}}}. \tag{67}$$

The $\beta_{root}$-values are maximized to 0.975. Using $\beta_{root}$ we can calculate the fraction of roots in each soil layer

$$Fr_{root\_n} = (1 - \beta_{root\_n})^{z_{\theta n}}, \tag{68}$$

which is used in the calculation of the vegetation surface resistance. According to Canadell et al. (1996) plants have the ability to compensate for dry conditions at a certain root level by increasing the efficiency of water uptake at other levels. This effect is accounted for as

$$\begin{cases} Fr_{root\_n} = & SWA_n Fr_{root\_n}, \\ Fr_{root\_n+1} = & Fr_{root\_n+1} + (1 - SWA_n) Fr_{root\_n}), \end{cases} \tag{69}$$

where $n$ represents soil layers 1 and 2 and $SWA$ is the soil-water availability defined as

$$SWA = \frac{\theta - \theta_{wi}}{\theta_{fc} - \theta_{wi}}. \tag{70}$$

## 6.3 Lake-depth database

The fractional area of the lakes and their area-weighted depth for each category are specified by combing the information on the lake depth from the database developed by Kourzeneva (2010) and the lake fraction information from ECOCLIMAP (Masson et al., 2003). The first version of the lake-depth database used in RCA4 was developed in May 2006. It provides reasonable coverage for most of Europe (Kourzeneva, 2010). When no information on the lake depth is available but the ECOCLIMAP data indicates that lakes are present within a grid box, a default depth of 10 m is used.

**Acknowledgments:**

The RCA4 simulations performed during the development phase of the code were conducted on resources provided by the Swedish National Infrastructure for Computing (SNIC) and computing resource Tornado funded with a grant from the Knut and Alice Wallenberg foundation, all housed at the National Supercomputer Centre (NSC) at Linköping University.

The surface code development has been supported through funding from

- the Mistra Swedish Research Programme for Climate, Impacts and Adaptation (Mistra-SWECIA)
- the Lund University Strategic Research Area Modelling the Regional and Global Earth System (MERGE)
- the European Union's Seventh Programme for research, technological development and demonstration under the following projects (grant agreement number): CLARIS-LPB (212492), GENESIS (226536)
- the Visby Programme at the Swedish Institute through the project "Lakes and regional climate", specially related to the implementation of FLake in RCA4
- the Swedish Research Council Formas under the ADSIMNOR project
- the Swedish Research Council Formas under the project "Towards tools for the assessment of coupled changes in regional climate, ecosystem and land use"

# A Aerodynamic resistances within the forest

The parameterisation of the bulk aerodynamic resistance $r_b = 1/g_b$ is based on Choudhury and Monteith (1988), where the conductance between the canopy and the canopy air, $g_b$, is defined as

$$g_b = \frac{2LAIa}{\alpha'}\left(\frac{u_{for}}{lw}\right)^{1/2}[1-\exp(-\alpha'/2)]. \tag{71}$$

The conductance is modified with a free convection correction according to Sellers et al. (1986)

$$g_b = g_b + \frac{LAI}{890}\left(\frac{T_{forc}-T_{fora}}{lw}\right)^{1/4}. \tag{72}$$

The aerodynamic resistance $r_d$ is based on Choudhury and Monteith (1988)

$$r_d = \frac{z_{for}\exp(\alpha)}{\alpha K(z_{for})}[\exp(-\alpha z'_0/z_{for}) - \exp(-\alpha(d+z_0)/z_{for})], \tag{73}$$

where

$$K(z_{for}) = k(z_{for}-d)u_{*for} = \frac{k^2(z_{for}-d)u}{\ln\frac{z_{for}-d}{z_0}}. \tag{74}$$

The displacement height is defined as (Choudhury and Monteith, 1988):

$$d = 1.1z_{for}\ln[1+(c_dLAI_f)^{1/4}] \tag{75}$$

where the leaf drag coefficient $c_d$ is defined as (Sellers et al., 1996):

$$c_d = 1.328\left[\frac{2}{\mathrm{Re}^{1/2}}\right] + 0.45\left[\frac{1}{\pi}(1-\chi_L)\right]^{1.6} \tag{76}$$

where $\chi_L$ is the Ross-Goudriaan leaf angle distribution function, which has been estimated according to Monteith (1975) (see Table 4), and Re is the Reynolds number defined as

$$\mathrm{Re} = \frac{u_l lw}{\upsilon}. \tag{77}$$

The unstable transfer correction for $r_d = r_d/\psi_H$ according to Sellers et al. (1986), where

$$\psi_H = \left[1+9\frac{T_{fors}-T_{fora}}{T_{fors}u^2_{for}}z_{for}\right]^{1/2}. \tag{78}$$

For the estimations of $r_b$ and $r_d$ the friction velocity at the forest tile, $u_{*for}$, is needed as well as the wind speed at the top of the forest, i.e. $u_{for}$ at $z_{for}$. $u_{*for}$ is estimated from the drag coefficient of momentum calculated as in Equation 3 but with $z_{0h}$ replaced by $z_{0m}$. $u_{for}$ is then reached in two steps: firstly the wind speed $u_{trans}$ at a transition level $z_{trans}$, located between $z_{am}$ and $z_{for}$, is calculated as

$$u(z_{trans}) = \frac{u_{*for}}{k}\left[\ln\frac{z_{trans}-d}{z_{0m}} - \Psi_m\left(\frac{z_{trans}-d}{L}\right)\right], \tag{79}$$

where $z_{trans}$ is defined as

$$z_{trans} = z_{for} + 11.785 z_{0m}. \tag{80}$$

Secondly, $u_{for} = u(z_{trans}) - G_2\Delta u(z_{trans}, z_{for})$, where $\Delta u(z_{trans}, z_{for}) = u(z_{trans}) - u(z_{for})$ and $G_2$ is an adjustment factor which is equal to 0.75 according to Xue et al. (1991).

Table 4: Surface independent parameters

| Symbol | Definition | Unit | Value | Reference | Comment |
|---|---|---|---|---|---|
| $g$ | Acceleration of gravity | m s$^{-2}$ | 9.81 | | |
| $G_2$ | Adjustment factor | - | 0.75 | Xue et al. (1991) | Eq. 13 |
| $k$ | von Karman constant | - | 0.4 | | |
| $a$ | | m s$^{-1/2}$ | 0.01 | Choudhury and Monteith (1988) | Eq. 26 |
| $\alpha'$ | attenuation coeff. for wind | - | 3 | Choudhury and Monteith (1988) | p 386 |
| $lw$ | leaf width | m | 0.02 | | |
| $\alpha$ | attenuation coeff. for mom. | - | 2 | Choudhury and Monteith (1988) | p 386 |
| $z_0'$ | roughness of soil surface | m | 0.007 | | |
| $\chi_L$ | Ross-Goudriaan leaf angle dist. | - | 0.12 | Monteith (1975) | p 26 |
| $u_l$ | Typical local wind speed | m s$^{-1}$ | 1 | Sellers et al. (1996) | Eq. B7 |
| $\upsilon$ | Kinematic viscos. of air | m$^2$ s$^{-1}$ | $0.15\cdot10^{-4}$ | | |

# B Snow density and snow albedo

## B.1 Snow density

The density of the snow increases exponentially with time towards a maximum value as long as no fresh snow is added by snowfall. The total density of the snow pack is a weighted value of the dry snow and of the liquid water content. Assuming that we have the density of the dry snow calculated, $\rho_{snd}$, which compare to the water equivalent of the dry snow, $sn_d$, we can combine that with any snowfall, $F$, during the time step to a temporary new dry snow density

$$\rho^*_{snd} = \frac{sn^\tau_d\rho^\tau_{snd} + (\Delta t F/\rho_w)\rho_{snmin}}{sn^\tau_d + (\Delta t F/\rho_w)}, \tag{81}$$

where $\rho_{snmin} = 100$ kg m$^{-3}$ is the minimum density of dry snow. The new value of the dry snow density becomes

$$\rho^{\tau+1}_{snd} = (\rho^*_{snd} - \rho_{snmax})\exp(-\tau_f\Delta t/\tau_1) + \rho_{snmax}, \tag{82}$$

where $\rho_{snmax} = 300$ kg m$^{-3}$ is the maximum density of dry snow. The time scales $\tau_1 = 86400$ s and $\tau_f = 0.24$ give an e-folding time of about 4 days. Combining the new dry snow density with the liquid water content in the snow gives the total density of the snow

$$\rho_{sn}^{\tau+1} = \Delta_{snd}^{\tau+1}\rho_{snd}^{\tau+1} + (1-\Delta_{snd}^{\tau+1})\rho_w, \tag{83}$$

where $\Delta_{snd}$ is the fraction of dry snow to total snow, i.e. $\Delta_{snd} = (sn - w_{sn})/sn$.

## B.2 Snow albedo

The net radiation balance at the surface for open land snow is given by $Rn_{sn} = (1-\alpha_{sn})S\downarrow + \varepsilon_{sn}(L\downarrow - \sigma T_{sn}^4)$, where the snow albedo, $\alpha_{sn}$, for open-land snow is a prognostic variable. The albedo for snow in the forest is set constant to 0.5.

The parameterisation of snow albedo evolution is divided into three main cases; snow fall situations, melting conditions and the rest (no snow fall and no melting). In the case of snow fall we distinguish between melting and non-melting conditions.

- For snow-fall events (snow fall intensity exceeds 0 kg m$^{-2}$ s$^{-1}$)
  - and melting conditions ($sn_{mel} > 0$)

$$\begin{cases} \alpha_{sn}^{*} = & \left(\frac{F_{sn} f_{sn2am}}{A_{opl}+A_{sn}}\right)^{f_{frsn}} \\ \alpha_{sn}^{\tau+1} = & \alpha_{sn}^{\tau}(1-\alpha_{sn}^{*}) + \alpha_{sn,melt}\alpha_{sn}^{*} \end{cases} \tag{84}$$

  - and non-melting conditions ($sn_{mel} = 0$)

$$\begin{cases} \alpha_{sn}^{*} = & \left(\frac{F_{sn} f_{sn2af}}{A_{opl}+A_{sn}}\right)^{f_{frsn}} \\ \alpha_{sn}^{\tau+1} = & \min\left[\alpha_{sn,max}, \alpha_{sn}^{\tau}(1-\alpha_{sn}^{*}) + \alpha_{sn,freeze}\alpha_{sn}^{*}\right] \end{cases} \tag{85}$$

- For conditions with no snow fall but melting ($sn_{mel} > 0$)

$$\begin{cases} \alpha_{sn}^{*} = & \max\left\{\alpha_{sn,melt}, \alpha_{sn}^{\tau} - \left[(\alpha_{sn,max} - \alpha_{sn,melt})\frac{sn_{mel}}{f_{albdec}*(A_{opl}+A_{sn})}\right]\right\} \\ \alpha_{sn}^{\tau+1} = & \min\left[\alpha_{sn}^{*}, (\alpha_{sn}^{\tau} - \alpha_{sn,min})\exp(-\tau_{fsn}\frac{\Delta t}{\tau_{1sn}}) + \alpha_{sn,min}\right] \end{cases} \tag{86}$$

- For conditions with no snow fall and no melting

$$\alpha_{sn}^{\tau+1} = \alpha_{sn}^{\tau} - \frac{\tau_{asn}\Delta t}{\tau_{1sn}(1+0.01(T_{sn}-T_{melt})^4)} \tag{87}$$

where

$$\begin{cases} f_{sn2am} = 1000\dfrac{\alpha_{sn,max} - \alpha_{sn,min}}{\rho_{sn,min} Z_{sn,\alpha_{sn,max}}(\alpha_{sn,melt} - \alpha_{sn,min})} \\ f_{sn2af} = 1000\dfrac{\alpha_{sn,max} - \alpha_{sn,min}}{\rho_{sn,min} Z_{sn,\alpha_{sn,max}}(\alpha_{sn,target} - \alpha_{sn,min})} \end{cases} \tag{88}$$

and

$\alpha_{sn,target} = 0.9$ is a target albedo for resetting snow albedo at snow fall events, $Z_{sn,\alpha_{sn,max}} = 0.05$ m is the snow-layer depth that resets albedo to its maximum value, $f_{frsn} = 0.8$ is a scaling factor for fraction covered by fresh snow, $\alpha_{sn,melt} = 0.7$ is the maximum snow albedo at melting conditions and $f_{albdec} = 0.003$ m is the amount of snow melt that gives a decay to $\alpha_{sn,melt}$ from $\alpha_{sn,max}$.

# C Diagnostic quantities

## C.1 Near-surface temperature, humidity and wind

Except for prognostic variables at the surface and at atmospheric model levels there is a need to calculate diagnostic variables that correspond to common observed quantities. Some of the most important diagnostic variables are air temperature and specific humidity at 2m height ($T2m$ and $q2m$) and wind speed components at 10m height ($u10$ and $v10$). The calculation of these diagnostic variables for a given height $z$ are based on Monin-Obukhov similarity theory:

$$\begin{cases} u(z) = \frac{u_*}{k}\left[\ln\frac{z}{z_{0m}} - \Psi_m\left(\frac{z}{L}\right)\right] \\ v(z) = \frac{v_*}{k}\left[\ln\frac{z}{z_{0m}} - \Psi_m\left(\frac{z}{L}\right)\right] \\ T(z) = T_s + \frac{\theta_*}{k}\left[\ln\frac{z}{z_{0h}} - \Psi_h\left(\frac{z}{L}\right)\right] \\ q(z) = q_s + \frac{q_*}{k}\left[\ln\frac{z}{z_{0q}} - \Psi_q\left(\frac{z}{L}\right)\right] \end{cases} \tag{89}$$

where $u_*$ and $v_*$ are friction velocities, $\theta_*$ and $q_*$ are temperature and humidity scales, respectively, $k$ is the von Karman's constant, $z_{0m}$, $z_{0h}$ and $z_{0q}$ are roughness lengths for momentum, heat and humidity, respectively, $L$ is the Monin-Obukhov length, $T_s$ and $q_s$ are surface values, and $\Psi_x$ represents analytic stability functions for momentum, heat and humidity, respectively.

In RCA4 these equations are approximated to (Woetmann Nielsen, 1987):

Stable case:

$$\begin{cases} u(z) = \frac{u_*}{k}\ln\frac{z}{z_{0m}} + u_{am}\left[1 - \exp\left(-\frac{1}{kRi_{cr}}\frac{u_*}{u_{am}}\frac{z}{L}\right)\right] \\ v(z) = \frac{v_*}{k}\ln\frac{z}{z_{0m}} + v_{am}\left[1 - \exp\left(-\frac{1}{kRi_{cr}}\frac{v_*}{v_{am}}\frac{z}{L}\right)\right] \\ T(z) = T_s + \frac{\theta_*}{k}\ln\frac{z}{z_{0h}} + (T_{am} - T_s)\left[1 - \exp\left(-\frac{1}{kRi_{cr}}\frac{\theta_*}{T_{am}}\frac{z}{L}\right)\right] \\ q(z) = q_s + \frac{q_*}{k}\ln\frac{z}{z_{0q}} + (q_{am} - q_s)\left[1 - \exp\left(-\frac{1}{kRi_{cr}}\frac{q_*}{q_{am}}\frac{z}{L}\right)\right] \end{cases} \tag{90}$$

where $Ri_{cr} = 0.25$, $z_{0q} = z_{0h}$ and subindex $am$ represents lowest atmospheric model level.

Unstable case:

$$\begin{cases} u(z) = \frac{u_*}{k}\left[\ln\frac{z}{z_{0m}} - \left(\ln\frac{1+x^2}{2} + 2\ln\frac{1+x}{2} - 2\tan^{-1}x + \frac{\pi}{2}\right)\right] \\ v(z) = \frac{v_*}{k}\left[\ln\frac{z}{z_{0m}} - \left(\ln\frac{1+x^2}{2} + 2\ln\frac{1+x}{2} - 2\tan^{-1}x + \frac{\pi}{2}\right)\right] \\ T(z) = T_s + \frac{\theta_*}{k}\left[\ln\frac{z}{z_{0h}} - 2\ln\frac{1+y}{2}\right] \\ q(z) = q_s + \frac{q_*}{k}\left[\ln\frac{z}{z_{0q}} - 2\ln\frac{1+y}{2}\right] \end{cases} \tag{91}$$

where $x = (1 - 15z/L)^{1/4}$ and $y = (1 - 9z/L)^{1/2}$.

The Monin-Obukhov length is defined as

$$L = -\frac{u_*^3 T}{kg\overline{w'\theta'_v}} = \frac{u_*^3}{kgH_v/c_p}\frac{p_s - dph}{R_d} = \frac{u_*^3}{kgH_v/(\rho c_p)}T_{am} \tag{92}$$

where the buoyancy flux $H_v$ is defined as

$$H_v = H + 0.61 c_p T_{am} E / L_e. \tag{93}$$

$u10$, $v10$, $T2m$ and $q2m$ are all calculated separately for each tile. Any diagnostic values representing groups of tiles or the whole grid square are calculated as area averaged values.

## C.2 Potential evapotranspiration

Potential evapotranspiration ($PET$) is calculated using a definition and method proposed by FAO (Allen et al., 1998). The method is derived from the Penman-Monteith equation. Note that $PET$ is a crop climate variable rather than an energy/water flux variable.

The FAO potential evapotranspiration is the evapotranspiration from a hypothetical crop surface, actively growing, completely shading the ground, with adequate water and only influenced by the atmospheric conditions. Hence, conditions within the soil (e.g. water and temperature) does not limit evapotranspiration. The hypothetical crop surface has a uniform crop height of 0.12 m, a fixed surface resistance of 70 s $m^{-1}$ and an albedo of 0.23. $PET$ is expressed as:

$$PET = -\frac{0.408\Delta(R_{net} - G) + \gamma \frac{900}{T_{2m}+273} U_{2m}(e_s - e_a)}{\Delta + \gamma(1 + 0.34 U_{2m})} \tag{94}$$

where

$PET$, potential evapotranspiration (mm $day^{-1}$),
$R_{net}$, surface net radiation (MJ $m^{-2}$ $day^{-1}$),
$G$, soil heat flux (MJ $m^{-2}$ $day^{-1}$),
$T_{2m}$, air temperature at 2 m (°C),
$U_{2m}$, wind speed at 2m (m $s^{-1}$),
$e_s$, saturated vapor pressure (kPa),
$e_a$, actual vapor pressure (kPa),
$\Delta$, slope of the vapor presure curve (kPa $°C^{-1}$),
$\gamma$, psycrometric constant (kPa $°C^{-1}$).

The slope of the vapor pressure curve and psycrometric constant are given by:

$$\Delta = \frac{4098(0.6108 e^{\frac{17.27 T_{2m}}{T_{2m}+237.3}})}{(T_{2m} + 237.3)^2} \tag{95}$$

$$\gamma = \frac{C_p P}{\varepsilon L_e} = 0.665 \cdot 10^{-3} \tag{96}$$

where $C_p$ is the specific heat of air (MJ $kg^{-1}°C^{-1}$), $\varepsilon$ the molecular weight of water/dry air (=0.622) and $L_e$ is the latent heat of vaporization (MJ $kg^{-1}$).

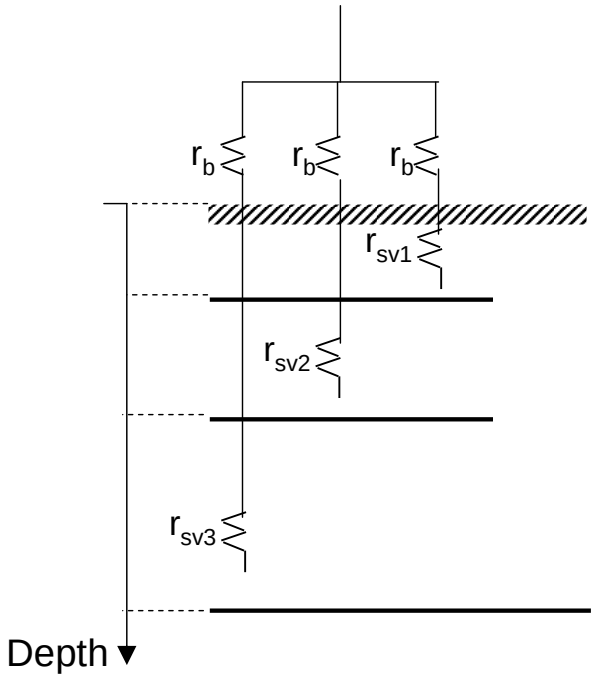


Figure 3: Principal sketch of the paralell coupling of individual soil resistances.

# D Numerical details

## D.1 Solving for $T_{fora}$ and $q_{fora}$

The heat fluxes in Equations 20 are functions of $T_{fora}$ or $q_{fora}$ but so are also the aerodynamic resistances included in the equations. Thus, the equilibrium value of $T_{fora}$ with respect to the temperatures $T_{forc}$, $T_{fors}$, $T_{forsn}$, and $T_{am}$ has to be solved for iteratively. $T_{fora}$ is solved from the relationship

$$H_{for} = H_{forc} + (1 - A_{forsn})H_{fors} + A_{forsn}H_{forsn} \tag{97}$$

which gives

$$T_{fora} = \frac{\frac{T_{am}}{r_{afor}} + \frac{(1-A_{forsn})T_{fors} + A_{forsn}T_{forsn}}{r_d} + \frac{T_{forc}}{r_b}}{\frac{1}{r_{afor}} + \frac{1}{r_d} + \frac{1}{r_b}}. \tag{98}$$

$q_{fora}$ is solved for in a similar manner with a corresponding equation for latent heat fluxes as the one for sensible heat fluxes in Equation 97.

## D.2 Weighting of surface resistances

The vegetation surface resistance according to Equation 10 is

$$r_{sv} = \frac{r_{svmin}}{\mathrm{LAI}} F_1 F_2^{-1} F_3^{-1} F_4^{-1} F_5^{-1}. \tag{99}$$

To account for different soil moisture and temperature conditions in different root layers the common factor $F_2^{-1}F_5^{-1}$ is calculated individually for each soil layer which in combination with the other

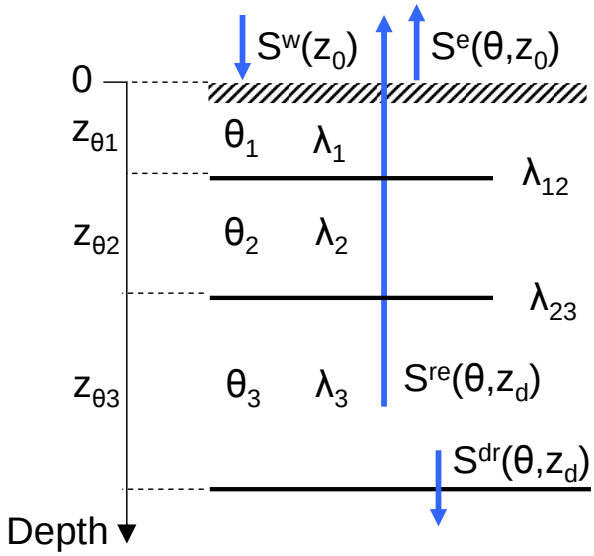


Figure 4: Principal sketch of the soil moisture layers.

factors actually gives different $r_{sv}$-values for each soil layer. As shown in Figure 3 these individual resistances are coupled in parallell, also including the aerodynamic resitance $r_b$ (forest case), which gives a weighted value according to

$$\begin{aligned}
\frac{1}{r_b+r_{sv}} &= \frac{Fr_{root1}}{r_b+r_{sv1}}+\frac{Fr_{root2}}{r_b+r_{sv2}}+\frac{Fr_{root3}}{r_b+r_{sv3}}= \\
&\frac{Fr_{root1}}{r_b+\frac{r_{svmin}}{\mathrm{LAI}}F_1F_3^{-1}F_4^{-1}F_{21}^{-1}F_{51}^{-1}}+\frac{Fr_{root2}}{r_b+\frac{r_{svmin}}{\mathrm{LAI}}F_1F_3^{-1}F_4^{-1}F_{22}^{-1}F_{52}^{-1}}+\frac{Fr_{root3}}{r_b+\frac{r_{svmin}}{\mathrm{LAI}}F_1F_3^{-1}F_4^{-1}F_{23}^{-1}F_{53}^{-1}}= \\
&\left\{\frac{1}{zqq}=\frac{r_{svmin}}{\mathrm{LAI}}F_1F_3^{-1}F_4^{-1}\right\}= \\
&\frac{Fr_{root1}zqqF_{21}F_{51}}{1+r_bzqqF_{21}F_{51}}+\frac{Fr_{root2}zqqF_{22}F_{52}}{1+r_bzqqF_{22}F_{52}}+\frac{Fr_{root3}zqqF_{23}F_{53}}{1+r_bzqqF_{23}F_{53}}
\end{aligned} \tag{100}$$

where $Fr_{root}$ represents the fractional distribution of roots between the three soil layers as described in Section 6.2.1.

## D.3 Solving the heat conduction

Once the fluxes are computed we solve the heat conduction for each tile, using the implicit method of Richtmeyer and Morton (1967). The degree of implicity is set to 0.5, except for the fast variables, $T_{forc}$, $T_{fors}$, $T_{forsn}$ and $T_{opls}$, which are treated fully implicitly.

## D.4 Solving the soil moisture

The modified Richards equation 57 becomes

$$\frac{\partial\theta}{\partial t}=\frac{\partial}{\partial z}\left(\lambda\frac{\partial\theta}{\partial z}\right)+S(\theta,z), \tag{101}$$

where $S(\theta,z)$ includes also a parameterization of the hydraulic conductivity term, $\partial\gamma/\partial z$, in Equation 57.

### D.4.1 The hydraulic diffusivity term

Considering the vertical discretization of layers as shown in Figure 4 we can rewrite Equation 101 as specified for layer 1 as

$$\frac{\partial\theta_1}{\partial t} = \left[\frac{\partial}{\partial z}\left(\lambda\frac{\partial\theta}{\partial z}\right)\right]_1 + S(\theta_1, z_{\theta 1}) = \frac{1}{z_{\theta 1}}\left(\lambda_{12}\left[\frac{\partial\theta}{\partial z}\right]_{12} - 0\right) + S(\theta_1, z_{\theta 1}). \tag{102}$$

Here

$$\left[\frac{\partial\theta}{\partial z}\right]_{12} = \frac{2(\theta_2-\theta_1)}{z_{\theta 1}+z_{\theta 2}} \tag{103}$$

and the hydraulic diffusivity at the boundary between layer 1 and 2, $\lambda_{12}$, is defined as

$$\frac{(z_{\theta 1}+z_{\theta 2})/2}{\lambda_{12}} = \frac{z_{\theta 1}/2}{\lambda_1} + \frac{z_{\theta 2}/2}{\lambda_2}. \tag{104}$$

Solving for $\lambda_{12}$ gives

$$\lambda_{12} = \frac{\lambda_1\lambda_2(z_{\theta 1}+z_{\theta 2})}{\lambda_1 z_{\theta 2}+\lambda_2 z_{\theta 1}}. \tag{105}$$

The equations for the three layers for the first term on the RHS of Equation 102 become

$$\begin{cases} \left[\frac{\partial}{\partial z}\left(\lambda\frac{\partial\theta}{\partial z}\right)\right]_1 = \frac{1}{z_{\theta 1}}\left(\lambda_{12}\left[\frac{\partial\theta}{\partial z}\right]_{12} - 0\right) \\ \left[\frac{\partial}{\partial z}\left(\lambda\frac{\partial\theta}{\partial z}\right)\right]_2 = \frac{1}{z_{\theta 2}}\left(\lambda_{23}\left[\frac{\partial\theta}{\partial z}\right]_{23} - \lambda_{12}\left[\frac{\partial\theta}{\partial z}\right]_{12}\right) \\ \left[\frac{\partial}{\partial z}\left(\lambda\frac{\partial\theta}{\partial z}\right)\right]_3 = \frac{1}{z_{\theta 3}}\left(0 - \lambda_{23}\left[\frac{\partial\theta}{\partial z}\right]_{23}\right) \end{cases} \tag{106}$$

Using the relationships in Equations 103 and 105 give

$$\begin{cases} \left[\frac{\partial}{\partial z}\left(\lambda\frac{\partial\theta}{\partial z}\right)\right]_1 = \frac{2\lambda_1\lambda_2}{z_{\theta 1}(\lambda_1 z_{\theta 2}+\lambda_2 z_{\theta 1})}(\theta_2-\theta_1) = \frac{\Lambda_{12}}{z_{\theta 1}}(\theta_2-\theta_1), \\ \left[\frac{\partial}{\partial z}\left(\lambda\frac{\partial\theta}{\partial z}\right)\right]_2 = \frac{1}{z_{\theta 2}}\left(\frac{2\lambda_2\lambda_3}{\lambda_2 z_{\theta 3}+\lambda_3 z_{\theta 2}}(\theta_3-\theta_2) - \frac{2\lambda_1\lambda_2}{\lambda_1 z_{\theta 2}+\lambda_2 z_{\theta 1}}(\theta_2-\theta_1)\right) = \frac{\Lambda_{23}}{z_{\theta 2}}(\theta_3-\theta_2) - \frac{\Lambda_{12}}{z_{\theta 2}}(\theta_2-\theta_1), \\ \left[\frac{\partial}{\partial z}\left(\lambda\frac{\partial\theta}{\partial z}\right)\right]_3 = -\frac{2\lambda_2\lambda_3}{z_{\theta 3}(\lambda_2 z_{\theta 3}+\lambda_3 z_{\theta 2})}(\theta_3-\theta_2) = -\frac{\Lambda_{23}}{z_{\theta 3}}(\theta_3-\theta_2). \end{cases} \tag{107}$$

### D.4.2 The source/sink term

The source/sink term for the three layers, respectively, becomes

$$\begin{cases} S(\theta_1, z_{\theta 1}) = S^w(z_0) - S^e(\theta_1, z_0) - S^{re}(\theta_1, z_{\theta 1}) - S^{dr}(\theta_1, z_{\theta 1}) - S^{srf}(z_{\theta 1}), \\ S(\theta_2, z_{\theta 2}) = S^{dr}(\theta_1, z_{\theta 1}) - S^{re}(\theta_2, z_{\theta 2}) - S^{dr}(\theta_2, z_{\theta 2}), \\ S(\theta_3, z_{\theta 3}) = S^{dr}(\theta_2, z_{\theta 2}) - S^{re}(\theta_3, z_{\theta 3}) - (1 - A_{wet}) S^{dr}(\theta_3, z_{\theta 3}), \end{cases} \tag{108}$$

where the different terms represent, respectively, supply of water at the soil surface, $S^w(z_0)$, evaporation/condensation at the soil surface, $S^e(\theta, z_0)$, loss due to root extraction, $S^{re}(\theta, z_d)$, and drainage/runoff, $S^{dr}(\theta, z_d)$, at each soil layer/interface $z_d$. For wetland conditions a surface runoff, as a residual term, is introduced, $S^{srf}(z_{\theta 1})$. The deep runoff, $S^{dr}(\theta_3, z_{\theta 3})$, is reduced as a function of the fraction of wetland, $A_{wet}$, where the wetland fraction in this example can represent values in the range 0–100%.

For open land and forest, respectively, $S^w(z_0)$ is defined as

$$\begin{cases} S^w(z_0)_{opl} = zrsfl * zfrop/(zfrop + zsnw) * (zrainop - zfzbr + zmelbs) + zsn2sw/(1 - zcw) \\ S^w(z_0)_{for} = zrsfl * (1. - zfrsnfor) * (zrainf - zfzbrc + zmelbsc) + zsnc2sw * zcwinv \end{cases} \tag{109}$$

The drainage/runoff terms, given by Equation 59, become

$$\begin{cases} S^{dr}(\theta_1, z_{\theta 1}) = S^w(z_0) \left( \frac{\theta_1 - \theta_{wi}}{\theta_{fc} - \theta_{wi}} \right)^{\beta} \\ S^{dr}(\theta_2, z_{\theta 2}) = S^{dr}(\theta_1, z_{\theta 1}) \left( \frac{\theta_2 - \theta_{wi}}{\theta_{fc} - \theta_{wi}} \right)^{\beta} = S^w(z_0) \left( \frac{\theta_1 - \theta_{wi}}{\theta_{fc} - \theta_{wi}} \right)^{\beta} \left( \frac{\theta_2 - \theta_{wi}}{\theta_{fc} - \theta_{wi}} \right)^{\beta} \\ S^{dr}(\theta_3, z_{\theta 3}) = (1 - A_{wet}) S^{dr}(\theta_2, z_{\theta 2}) \left( \frac{\theta_3 - \theta_{wi}}{\theta_{fc} - \theta_{wi}} \right)^{\beta} = (1 - A_{wet}) S^{dr}(\theta_1, z_{\theta 1}) \left( \frac{\theta_2 - \theta_{wi}}{\theta_{fc} - \theta_{wi}} \right)^{\beta} \left( \frac{\theta_3 - \theta_{wi}}{\theta_{fc} - \theta_{wi}} \right)^{\beta} \end{cases} \tag{110}$$

### D.4.3 The numerical solution

The numerical solution of Richards Equation 101, using the implicit method of Richtmeyer and Morton (1967) where the degree of implicity is given by the factor $\alpha$, for a specific depth $d$ becomes

$$\frac{\theta_d^{\tau+1} - \theta_d^{\tau}}{\Delta t} = (1 - \alpha)\phi_d^{\tau} + \alpha \phi_d^{\tau+1}, \tag{111}$$

where

$$\phi_d = \left[ \frac{\partial}{\partial z} \left( \lambda \frac{\partial \theta}{\partial z} \right) \right]_d + S(\theta_d, z_{\theta d}). \tag{112}$$

The implicit term $\phi_d^{\tau+1}$ is defined as

$$\phi_d^{\tau+1} = \phi_d^{\tau} + \frac{\partial \phi_d}{\partial \theta_{d-1}} (\theta_{d-1}^{\tau+1} - \theta_{d-1}^{\tau}) + \frac{\partial \phi_d}{\partial \theta_d} (\theta_d^{\tau+1} - \theta_d^{\tau}) + \frac{\partial \phi_d}{\partial \theta_{d+1}} (\theta_{d+1}^{\tau+1} - \theta_{d+1}^{\tau}) \tag{113}$$

Using this expression in Equation 111 gives

$$\frac{\theta_d^{\tau+1}-\theta_d^{\tau}}{\Delta t}=\phi_d^{\tau}+\alpha\left[\frac{\partial\phi_d}{\partial\theta_{d-1}}(\theta_{d-1}^{\tau+1}-\theta_{d-1}^{\tau})+\frac{\partial\phi_d}{\partial\theta_d}(\theta_d^{\tau+1}-\theta_d^{\tau})+\frac{\partial\phi_d}{\partial\theta_{d+1}}(\theta_{d+1}^{\tau+1}-\theta_{d+1}^{\tau})\right]. \quad (114)$$

The $\phi$-equations become

$$\begin{cases}\phi_1=\dfrac{\Lambda_{12}}{z_{\theta 1}}(\theta_2-\theta_1)+S^w(z_0)-S^e(\theta_1,z_0)-S^{re}(\theta_1,z_{\theta 1})-S^{dr}(\theta_1,z_{\theta 1}),\\ \phi_2=\dfrac{\Lambda_{23}}{z_{\theta 2}}(\theta_3-\theta_2)-\dfrac{\Lambda_{12}}{z_{\theta 2}}(\theta_2-\theta_1)+S^{dr}(\theta_1,z_{\theta 1})-S^{dr}(\theta_2,z_{\theta 2})-S^{re}(\theta_2,z_{\theta 2})\\ \phi_3=-\dfrac{\Lambda_{23}}{z_{\theta 3}}(\theta_3-\theta_2)+S^{dr}(\theta_2,z_{\theta 2})-(1-A_{wet})S^{dr}(\theta_3,z_{\theta 3})-S^{re}(\theta_3,z_{\theta 3}),\end{cases} \quad (115)$$

where the terms $S^e(\theta_1,z_0)$ and $S^{re}(\theta_1,z_{\theta 1})$ are given from Equations 29 and 28, respectively, using open land as an example

$$\begin{cases}S^e(\theta_1,z_0)=\frac{1}{L_e\rho_w}E_{opls}\\ S^{re}(\theta_1,z_{\theta 1})=\frac{1}{L_e\rho_w}E_{oplv}.\end{cases} \quad (116)$$

Note that we have omitted the surface runoff term related to wetlands, $S^{srf}(z_{\theta 1})$ introduced in Equation 108, since it will be considered as a residual term in the end.

Using the expressions in Equations 110 in Equations 115 give

$$\begin{cases}\phi_1=\dfrac{\Lambda_{12}}{z_{\theta 1}}(\theta_2-\theta_1)+S^w(z_0)\left(1-\left(\dfrac{\theta_1-\theta_{wi}}{\theta_{fc}-\theta_{wi}}\right)^{\beta}\right)-S^e(\theta_1,z_0)-S^{re}(\theta_1,z_{\theta 1}),\\ \phi_2=\dfrac{\Lambda_{23}}{z_{\theta 2}}(\theta_3-\theta_2)-\dfrac{\Lambda_{12}}{z_{\theta 2}}(\theta_2-\theta_1)+S^w(z_0)\left(\dfrac{\theta_1-\theta_{wi}}{\theta_{fc}-\theta_{wi}}\right)^{\beta}\left(1-\left(\dfrac{\theta_2-\theta_{wi}}{\theta_{fc}-\theta_{wi}}\right)^{\beta}\right)-S^{re}(\theta_2,z_{\theta 2})\\ \phi_3=-\dfrac{\Lambda_{23}}{z_{\theta 3}}(\theta_3-\theta_2)+S^{dr}(\theta_1,z_{\theta 1})\left(\dfrac{\theta_2-\theta_{wi}}{\theta_{fc}-\theta_{wi}}\right)^{\beta}\left(1-\left(\dfrac{\theta_3-\theta_{wi}}{\theta_{fc}-\theta_{wi}}\right)^{\beta}\right)-S^{re}(\theta_3,z_{\theta 3}),\end{cases} \quad (117)$$

For an implicit solution we need the derivatives of the terms in Equation 117 with respect to $\theta$. The fast-response terms are those connected to drainage. Thus, we apply a semi-implicit solution only considering the derivatives of the drainage terms. We also assume $\beta=2$.

$$\left\{\begin{array}{l}
\dfrac{\partial\phi_1}{\partial\theta_1} = -S^w(z_0)\dfrac{2}{(\theta_{fc}-\theta_{wi})^2}(\theta_1-\theta_{wi}) \\
\dfrac{\partial\phi_2}{\partial\theta_1} = S^w(z_0)\left(1-\left(\dfrac{\theta_2-\theta_{wi}}{\theta_{fc}-\theta_{wi}}\right)^{\beta}\right)\dfrac{2}{(\theta_{fc}-\theta_{wi})^2}(\theta_1-\theta_{wi}) \\
\dfrac{\partial\phi_2}{\partial\theta_2} = -S^w(z_0)\left(\dfrac{\theta_1-\theta_{wi}}{\theta_{fc}-\theta_{wi}}\right)^{\beta}\dfrac{2}{(\theta_{fc}-\theta_{wi})^2}(\theta_2-\theta_{wi}) \\
\dfrac{\partial\phi_3}{\partial\theta_2} = S^{dr}(z_{\theta_1,\theta 1})\left(1-\left(\dfrac{\theta_3-\theta_{wi}}{\theta_{fc}-\theta_{wi}}\right)^{\beta}\right)\dfrac{2}{(\theta_{fc}-\theta_{wi})^2}(\theta_2-\theta_{wi}) \\
\dfrac{\partial\phi_3}{\partial\theta_3} = -S^{dr}(z_{\theta_1,\theta 1})\left(\dfrac{\theta_2-\theta_{wi}}{\theta_{fc}-\theta_{wi}}\right)^{\beta}\dfrac{2}{(\theta_{fc}-\theta_{wi})^2}(\theta_3-\theta_{wi})
\end{array}\right. \tag{118}$$

Putting these expressions into Equation 114 gives

$$\left\{\begin{array}{lll}
\theta_1^{\tau+1} = & \theta_1^{\tau}+\Delta t\left\{\phi_1^{\tau}+\alpha\left[\dfrac{\partial\phi_1}{\partial\theta_1}(\theta_1^{\tau+1}-\theta_1^{\tau})\right]\right\} \\
\theta_2^{\tau+1} = & \theta_2^{\tau}+\Delta t\left\{\phi_2^{\tau}+\alpha\left[\dfrac{\partial\phi_2}{\partial\theta_1}(\theta_1^{\tau+1}-\theta_1^{\tau})+\dfrac{\partial\phi_2}{\partial\theta_2}(\theta_2^{\tau+1}-\theta_2^{\tau})\right]\right\} \\
\theta_3^{\tau+1} = & \theta_3^{\tau}+\Delta t\left\{\phi_3^{\tau}+\alpha\left[\dfrac{\partial\phi_3}{\partial\theta_2}(\theta_2^{\tau+1}-\theta_2^{\tau})+\dfrac{\partial\phi_3}{\partial\theta_3}(\theta_3^{\tau+1}-\theta_3^{\tau})\right]\right\}
\end{array}\right. \tag{119}$$

The implicit solution is given by $A\theta^{\tau+\mathbf{1}} = \mathbf{b}$ where

$$\theta^{\tau+\mathbf{1}} = \left[\begin{array}{c} \theta_1^{\tau+1} \\ \theta_2^{\tau+1} \\ \theta_3^{\tau+1} \end{array}\right], \tag{120}$$

and the 3x3 matrix $A$ is

$$A = \left[\begin{array}{ccc}
1-\alpha\Delta t\dfrac{\partial\phi_1}{\partial\theta_1} & 0 & 0 \\
-\alpha\Delta t\dfrac{\partial\phi_2}{\partial\theta_1} & 1-\alpha\Delta t\dfrac{\partial\phi_2}{\partial\theta_2} & 0 \\
0 & -\alpha\Delta t\dfrac{\partial\phi_3}{\partial\theta_2} & 1-\alpha\Delta t\dfrac{\partial\phi_3}{\partial\theta_3}
\end{array}\right], \tag{121}$$

and the vector $\mathbf{b}$ is

$$\mathbf{b} = \left[\begin{array}{c}
\theta_1^{\tau}+\Delta t\left\{\phi_1^{\tau}-\alpha\dfrac{\partial\phi_1}{\partial\theta_1}\theta_1^{\tau}\right\} \\
\theta_2^{\tau}+\Delta t\left\{\phi_2^{\tau}-\alpha\left[\dfrac{\partial\phi_2}{\partial\theta_1}\theta_1^{\tau}+\dfrac{\partial\phi_2}{\partial\theta_2}\theta_2^{\tau}\right]\right\} \\
\theta_3^{\tau}+\Delta t\left\{\phi_3^{\tau}-\alpha\left[\dfrac{\partial\phi_3}{\partial\theta_2}\theta_2^{\tau}+\dfrac{\partial\phi_3}{\partial\theta_3}\theta_3^{\tau}\right]\right\}
\end{array}\right]. \tag{122}$$

# E ECOCLIMAP specifications

Table 5: ECOCLIMAP parameters

| Variable | Description | nn | ECOCLIMAP file |
|---|---|---|---|
| lai_t1 | LAI open land | 1 | time_of_year( lai.time.t01.NSCALE ) |
| lai_t2 | LAI conif forest | 2 | time_of_year( lai.time.t02.NSCALE ) |
| lai_t3 | LAI broad-leaf forest | 3 | time_of_year( lai.time.t03.NSCALE ) |
| z0_t1 | roughness length open land | 4 | time_of_year( z0.time.t01.NSCALE ) |
| z0_t2 | roughness length conif forest | 5 | time_of_year( z0.time.t02.NSCALE ) |
| z0_t3 | roughness length broad-leaf forest | 6 | time_of_year( z0.time.t03.NSCALE ) |
| emis_t1 | emissivity open land | 7 | time_of_year( emis.time.t01.NSCALE ) |
| alb_t1 | albedo open land | 8 | time_of_year( alb.time.t01.NSCALE ) |
| veg_t1 | vegetation cover open land | 9 | time_of_year( veg.time.t01.NSCALE ) |
| frland | fraction land | 10 | 1 - F_wat.NSCALE |
| alb_soil | albedo of bare soil | 11 | albedo_soil.NSCALE |
| clay | percentage of clay | 12 | clay.NSCALE |
| sand | percentage of sand | 13 | sand.NSCALE |
| frac_t1 | fraction open land | 14 | frac_tile01.NSCALE |
| frac_t2 | fraction conif forest | 15 | frac_tile02.NSCALE |
| frac_t3 | fraction broad-leaf forest | 16 | frac_tile03.NSCALE |
| alb_t2 | albedo conif forest | 17 | alb.07.t02.NSCALE |
| alb_t3 | albedo broad-leaf forest | 18 | alb.07.t03.NSCALE |
| emis_t2 | emissivity conif forest | 19 | emis.07.t02.NSCALE |
| emis_t3 | emissivity broad-leaf forest | 20 | emis.07.t03.NSCALE |
| veg_t2 | vegetation cover conif forest | 21 | veg.07.t02.NSCALE |
| veg_t3 | vegetation cover broad-leaf forest | 22 | veg.07.t03.NSCALE |
| droot_t1 | root depth open land | 23 | d_root.t01.NSCALE |
| droot_t2 | root depth conif forest | 24 | d_root.t02.NSCALE |
| droot_t3 | root depth broad-leaf forest | 25 | d_root.t03.NSCALE |
| dsoil_t1 | soil depth open land | 26 | d_soil.t01.NSCALE |
| dsoil_t2 | soil depth conif forest | 27 | d_soil.t02.NSCALE |
| dsoil_t3 | soil depth broad-leaf forest | 28 | d_soil.t03.NSCALE |
| rsmin_t1 | minimum surface resistance open land | 29 | rsmin.t01.NSCALE |
| rsmin_t2 | minimum surface resistance conif forest | 30 | rsmin.t02.NSCALE |
| rsmin_t3 | minimum surface resistance | 31 | rsmin.t03.NSCALE |
| alb_veg_t1 | albedo vegetation open land | 32 | albedo_veg.t01.NSCALE |
| alb_veg_t2 | albedo vegetation conif forest | 33 | albedo_veg.t02.NSCALE |
| alb_veg_t3 | albedo vegetation | 34 | albedo_veg.t03.NSCALE |
| texture | texture according to texture triangle | 35 | Processed info see "Texture" below |
| minlai_t1 | annual min of LAI open land | 36 | min( lai.time.t01.NSCALE ) |
| minlai_t2 | annual min of LAI conif forest | 37 | min( lai.time.t02.NSCALE ) |
| minlai_t3 | annual min of LAI broad-leaf forest | 38 | min( lai.time.t03.NSCALE ) |
| maxlai_t1 | annual max of LAI open land | 39 | max( lai.time.t01.NSCALE ) |
| maxlai_t2 | annual max of LAI conif forest | 40 | max( lai.time.t02.NSCALE ) |
| maxlai_t3 | annual max of LAI broad-leaf forest | 41 | max( lai.time.t03.NSCALE ) |
| frac_lake | fraction of lake | 42 | F_lake.NSCALE |
| soil_carb | soil carbon | 43 | soil_carb.NSCALE |

Table 6: Soil texture classes

| **Number** | **Texture class** | $\theta_{sat}$ ($m^3m^{-3}$) | $\theta_{fc}$ ($m^3m^{-3}$) | $\theta_{wi}$ ($m^3m^{-3}$) | $\psi_{sat}$ (m) | $\gamma_{sat}$ (m $s^{-1}$) | $b$ (-) | $cq$ (-) |
|---|---|---|---|---|---|---|---|---|
| 1 | silty loam | 0.485 | 0.369 | 0.179 | 0.786 | 7.2 | 5.3 | 0.25 |
| 2 | sand | 0.395 | 0.174 | 0.068 | 0.121 | 176 | 4.05 | 0.92 |
| 3 | silty clay loam | 0.477 | 0.357 | 0.218 | 0.356 | 1.7 | 7.75 | 0.1 |
| 4 | loam | 0.451 | 0.314 | 0.155 | 0.478 | 6.95 | 5.39 | 0.4 |
| 5 | clay loam | 0.476 | 0.391 | 0.25 | 0.63 | 2.45 | 8.52 | 0.35 |
| 6 | sandy loam | 0.435 | 0.249 | 0.114 | 0.218 | 34.7 | 4.9 | 0.6 |
| 7 | silty clay | 0.492 | 0.409 | 0.283 | 0.49 | 1.03 | 10.4 | 0.1 |
| 8 | sandy clay loam | 0.42 | 0.299 | 0.175 | 0.299 | 6.3 | 7.12 | 0.6 |
| 9 | loamy sand | 0.41 | 0.179 | 0.075 | 0.09 | 156 | 4.38 | 0.82 |
| 10 | clay | 0.482 | 0.4 | 0.286 | 0.405 | 1.28 | 11.4 | 0.25 |
| 11 | silt | 0.485 | 0.369 | 0.179 | 0.786 | 7.2 | 5.3 | 0.1 |
| 12 | sandy clay | 0.426 | 0.316 | 0.219 | 0.153 | 2.17 | 10.4 | 0.52 |

# References


Allen, R. G., Pereira, L. S., Raes, D., Smith, M., 1998. Crop evapotranspiration: Guidelines for computing crop water requirements. FAO irrigation and drainage paper 56, FAO, iSBN 92-5-104219-5.

Beljaars, A. C. M., Viterbo, P., 1994. The sensitivity of winter evaporation to the formulation of aerodynamic resistance in the ECMWF model. Boundary-Layer Meteorol. 71, 135–149.

Bergström, S., Graham, L. P., 1998. On the scale problem in hydrological modelling. J. Hydrology 211, 253–265.

Bringfelt, B., Räisänen, J., Gollvik, S., Lindström, G., Graham, L. P., Ullerstig, A., 2001. The land surface treatment for the Rossby Centre regional atmosphere climate model - version 2. Reports of Meteorology and Climatology 98, SMHI, SE-601 76 Norrköping, Sweden.

Canadell, J., Jackson, R. B., Ehleringer, J. B., Mooney, H. A., Sala, O. E., Schulze, E.-D., 1996. Maximum rooting depth of vegetation types at the global scale. Oecologia 108, 583–595, doi: 10.1007/BF00329030.

Chen, F., Janjić, Z., Mitchell, K., 1997. Impact of atmospheric surface-layer parameterizations in the new land-surface scheme of the NCEP Eta model. Boundary-Layer Meteorol. 85, 391–421.

Choudhury, B. J., Monteith, J. L., 1988. A four-layer model for the heat budget of homogeneous land surfaces. Q. J. R. Meteorol. Soc. 114, 373–398.

Deardorff, J. W., 1978. Efficient prediction of ground surface temperature and moisture, with inclusion of a layer of vegetation. J. Geophys. Res. 83, 1889–1903.

Dickinson, R. E., 1984. Modeling evapotranspiration for three dimensional global climate models. Climate Processes and Climate Sensitivity. Geophys. Monogr. 29, 58–72.

FAO-Unesco (Ed.), 1981. Soil map of the world: Vol. 5, Europe. Unesco-Paris.

Global Soil Data Task, 2000. Global gridded surfaces of selected soil characteristics (IGBPDIS). International geosphere-biosphere programme. Data and information services. http://www.daac.ornl.gov/, doi:10.3334/ORNLDAAC/569.

Hagemann, S., Botzet, M., Dümenil, L., Machenhauer, B., 1999. Derivation og global GCM boundary conditions from 1 km land use satellite data. Tech. Rep. 289, Max-Planck-Institute for Meteorology, Hamburg, Germany.

Hillel, D., 1980. Fundamentals of Soil Physics. Academic Press, New York.

Jackson, R. B., Canadell, J., Ehleringer, J. R., Mooney, H. A., Sala, O. E., Schulze, E. D., 1996. A global analysis of root distributions for terrestrial biomes. Oecologia 108, 389–411.

Jarvis, P. G., 1976. The interpretation of the variations in leaf water potential and stomatal conductance found in canopies in the field. Phil. Trans. Roy. Soc. London B273, 593–610.

Kondo, J., Yamazaki, T., 1990. A prediction model for snowmelt, snow surface temperature and freezing depth using a heat balance method. J. Appl. Meteor. 29, 375384, doi:http://dx.doi.org/10.1175/1520-0450(1990)029¡0375:APMFSS¿2.0.CO;2.

Kourzeneva, E. V., 2010. External data for lake parameterization in numerical weather prediction and climate modeling. Boreal Env. Res. 15, 165–177.

Lawrence, D. M., Slater, A. G., 2008. Incorporating organic soil into a global climate model. Clim. Dyn. 30, 145–160.

Lindström, G., Gardelin, M., 1999. A simple snow parameterization scheme intended for the RCA model based on the HBV runoff model. SWECLIM Newsletter 6, SMHI, Sweden, 16–20.

Lindström, G., Johansson, B., Persson, M., Gardelin, M., Bergström, S., 1997. Development and test of the distributed HBV-96 hydrological model. J. Hydrology 201, 272–288.

Louis, J. F., Tiedtke, M., Geleyn, J. F., 1981. A short history of the PBL parameterization at ECMWF. In: Workshop on Boundary Layer Parameterization. European Centre for Medium-Range Weather Forecasts, Reading, U.K.

Masson, V., Champeaux, J. L., Chauvin, F., Mériguet, C., Lacaze, R., 2003. A global database of land surface parameters at 1km resolution for use in meteorological and climate models. J. Climate 16, 1261–1282.

McCumber, M. C., Pielke, R. A., 1981. Simulation of the effects of surface fluxes of heat and moisture in a mesoscale numerical model 1. Soil layer. J. Geophys. Res. 86, 9,929–9,938.

Mironov, D., Heise, E., Kourzeneva, E., Ritter, B., Schneider, N., Terzhevik, A., 2010. Implementation of the lake parameterisation scheme flake into the numerical weather prediction model cosmo. Boreal Env. Res. 15, 218–230.

Mironov, D. V., 2008. Parameterization of lakes in numerical weather prediction. description of a lake model. COSMO Technical Report 11, Deutscher Wetterdienst, Offenbach am Main, Germany.

Monteith, J. L. (Ed.), 1975. Vegetation and the atmosphere. Vol. 1. Academic Press.

Noilhan, J., Planton, S., 1989. A simple parameterization of land surface processes for meteorological models. Mon. Wea. Rev. 117, 536–549.

Peters-Lidard, C. D., Blackburn, E., Liang, X., Wood, E. F., 1998. The effect of soil thermal conductivity parameterization on surface energy fluxes and temperatures. J. Atmos. Sci. 55, 1209–1224.

Richtmeyer, R. D., Morton, K. W., 1967. Difference Methods for Initial-Value Problems. Interscience Publishers.

Rutgersson, A., Smedman, A.-S., Omstedt, A., 2001. Measured and simulated latent and sensible heat fluxes at two marine sites in the Baltic Sea. Boundary-Layer Meteorology 99, 53–84.

Samuelsson, P., Bringfelt, B., Graham, L. P., 2003. The role of aerodynamic roughness for runoff and snow evaporation in land-surface schemes — comparison of uncoupled to coupled simulations. Global Planetary Change 38, 93–99.

Samuelsson, P., Gollvik, S., Ullerstig, A., 2006. The land-surface scheme of the Rossby Centre regional atmospheric climate model (RCA3). Report in Meteorology 122, SMHI, SE-601 76 Norrköping, Sweden.

Samuelsson, P., Kourzeneva, E., Mironov, D., 2010. The impact of lakes on the european climate as simulated by a regional climate model. Boreal Env. Res. 15, 113–129.

Sellers, P. J., Mintz, Y., Sud, Y. C., Dalcher, A., 1986. A simple biosphere model (SiB) for use within general ciculation models. J. Atmos. Sci. 43, 505–531.

Sellers, P. J., Randall, D. A., Collatz, G. J., Berry, J. A., Field, C. B., Dazlich, D. A., Zhang, C., Collelo, G. D., Bounoua, L., 1996. A revised land surface parameterization (SiB2) for atmospheric GCMs. Part I: Model formulation. J. Climate 9, 676–705.

Sitch, S., SMith, B., Prentice, I. C., Arneth, A., Bondeau, A., co authors, 2003. Evaluation of ecosystem dynamics, plant geography and terrestrial carbon cycling in the lpj dynamic vegetation model. Global Vhange Biol. 9, 161–185.

Smith, B., Prentice, I. C., Sykes, M. T., 2001. Representation of vegetation dynamics in modelling of the terrestrial ecosystems: comparing two contrasting approaches within european climate space. Global Ecol. Biogeog. 10, 621–637.

Smith, B., Samuelsson, P., Wramneby, A., Rummukainen, M., 2011. A model of the coupled dynamics of climate, vegetation and terrestrial ecosystem biogeochemistry for regional applications. Tellus 63, 87–106.

Strandberg, G., Bärring, L., Hansson, U., Jansson, C., Jones, C., Kjellström, K., Kolax, M., Kupiainen, M., Nikulin, G., Samuelsson, P., Ullerstig, A., Wang, S., 2014. CORDEX scenarios for Europe from the Rossby Centre regional climate model RCA4. Reports Meteorology and Climatology 999, SMHI, SE-601 76 Norrköping, Sweden.

Survey, U. G., 1996. Global 30 Arc-Second Elevation (GTOPO30) . https://lta.cr.usgs.gov/GTOPO30.

van den Hurk, B., Viterbo, P., 2003. The Torne-Kalix PILPS2E experiment as a test bed for modifications to the ECMWF land surface scheme. Global Planetary Change 38, 165–173.

van den Hurk, B. J. J. M., Viterbo, P., Beljaars, A. C. M., Betts, A. K., 2000. Offline validation of the ERA40 surface scheme. Technical Memorandum 295, ECMWF.

Verseghy, D. L., McFarlane, N. A., Lazare, M., 1993. CLASS – A Canadian land surface scheme for GCMs, II. Vegetation model and coupled runs. Int. J. Climatol. 13, 347–370.

Viterbo, P., Beljaars, A., Teixeira, J., 1999. The representation of soil moisture freezing and its impact on the stable boundary layer. Quart. J. Roy. Meteorol. Soc. 125, 2401–2426.

Wang, S., Dieterich, C., Döscher, R., Höglund, A., Hordoir, R., Meier, H., Samuelsson, P., Schimanke, S., 2015. Development and evaluation of a new regional coupled atmosphere-ocean model in the North Sea and Baltic Sea. Tellus A 67, 24284, doi: http://dx.doi.org/10.3402/tellusa.v67.24284.

Woetmann Nielsen, N., 1987. An approximate method for calculation of surface fluxes in an unstable atmospheric surface layer. HIRLAM Technical Note 1.

Wramneby, A., Smith, B., Samuelsson, P., 2010. Hot spots of vegetation-climate feedbacks under future greenhouse forcing in europe. J. Geophys. Res. 115, D21119.

Wu, M., Smith, B., Schurgers, G., Lindström, J., Rummukainen, M., Samuelsson, P., 2013. Vegetation-climate feedbacks causes reduced precipitation in cmip5 regional earth system model simulation over africa. In: Geophysical Research Abstracts. European Geosciences Union, Vienna, Austria.

Xue, Y., Sellers, P. J., Kinter, J. L., Shukla, J., 1991. A simplified Biosphere Model for Global Climate Studies. J. Climate 4, 345–364.

Zhang, W., Jansson, C., Miller, P., Smith, B., Samuelsson, P., 2014. Biogeophysical feedbacks enhances the arctic terrestrial carbon sink in regional earth system dynamics. Biogeosciences 11, 5503–5519.

Zilitinkevich, S., 1995. Non-local turbulent transport: Pollution dispersion aspects of coherent structure of convective flows. In: Power, H., Moussiopoulos, N., Brebbia, C. A. (Eds.), Air pollution III - Volume I. Air pollution theory and simulation. Computational Mechanics Publications, Southhampton, Boston, pp. 53–60.

Zinke, P. J., Stangenberger, A. G., Post, W. M., Emanuel, W. R., Olson, J. S., 1986. Worldwide organic carbon and nitrogen data. Tech. Rep. ONRL/CDIC-18, Carbon Dioxide Information Centre, Oak Ridge, Tenessee, doi:10.3334/CDIAC/lue.ndp018.

**I serien METEOROLOGI har tidigare utgivits**:

1985

1 Hagmarker, A. (1985)
Satellitmeteorologi.

2 Fredriksson, U., Persson, Ch., Laurin, S. (1985)
Helsingborgsluft.

3 Persson, Ch, Wern, L. (1985)
Spridnings- och depositionsberäkningar för avfallsförbränningsanläggningar i Sofielund och Högdalen.

4 Kindell, S. (1985)
Spridningsberäkningar för SUPRAs anläggningar i Köping.

5 Andersson, C., Kvick, T. (1985)
Vindmätningar på tre platser på Gotland. Utvärdering nr 1.

6 Kindell, S. (1985)
Spridningsberäkningar för Ericsson, Ingelstafabriken.

7 Fredriksson, U. (1985)
Spridningsberäkningar för olika plymlyft vid avfallsvärmeverket Sävenäs.

8 Fredriksson, U., Persson, Ch. (1985)
$NO_x$- och $NO_2$-beräkningar vid Vasaterminalen i Stockholm.

9 Wern, L. (1985)
Spridningsberäkningar för ASEA transformers i Ludvika.

10 Axelsson, G., Eklind, R. (1985)
Ovädret på Östersjön 23 juli 1985.

11 Laurin, S., Bringfelt, B. (1985)
Spridningsmodell för kväveoxider i gatumiljö.

12 Persson, Ch., Wern, L. (1985)
Spridnings- och depositionsberäkningar för avfallsförbränningsanläggning i Sofielund.

13 Persson, Ch., Wern, L. (1985)
Spridnings- och depositionsberäkningar för avfallsförbränningsanläggning i Högdalen.

14 Vedin, H., Andersson, C. (1985)
Extrema köldperioder i Stockholm.

15 Krieg, R., Omstedt, G. (1985)
Spridningsberäkningar för Volvos planerade bilfabrik i Uddevalla.

16 Kindell, S. Wern, L. (1985)
Luftvårdsstudie avseende industrikombinatet i Nynäshamn (koncentrations- och luktberäkningar).

17 Laurin, S., Persson, Ch. (1985)
Beräknad formaldehydspridning och deposition från SWEDSPANs spånskivefabrik.

18 Persson, Ch., Wern, L. (1985)
Luftvårdsstudie avseende industrikombinatet i Nynäshamn – depositionsberäkningar av koldamm.

19 Fredriksson, U. (1985)
Luktberäkningar för Bofors Plast i Ljungby, II.

20 Wern, L., Omstedt, G. (1985)
Spridningsberäkningar för Volvos planerade bilfabrik i Uddevalla - energicentralen.

21 Krieg, R., Omstedt, G. (1985)
Spridningsberäkningar för Volvos planerade bilfabrik i Uddevalla - kompletterande beräkningar för fabrikerna.

22 Karlsson, K.-G. (1985)
Information från Meteosat - forskningsrön och operationell tillämpning.

23 Fredriksson, U. (1985)
Spridningsberäkningar för AB Åkerlund & Rausings fabrik i Lund.

24 Färnlöf, S. (1985)
Radarmeteorologi.

25 Ahlström, B., Salomonsson, G. (1985)
Resultat av 5-dygnsprognos till ledning för isbrytarverksamhet vintern 1984-85.

26 Wern, L. (1985)
Avesta stadsmodell.

27 Hultberg, H. (1985)
Statistisk prognos av yttemperatur.

1986

1 Krieg, R., Johansson, L., Andersson, C. (1986)
Vindmätningar i höga master, kvartalsrapport 3/1985.

2 Olsson, L.-E., Kindell, S. (1986)
Air pollution impact assessment for the SABAH timber, pulp and paper complex.

3 Ivarsson, K.-I. (1986)
Resultat av byggväderprognoser - säsongen 1984/85.

4 Persson, Ch., Robertson, L. (1986)
Spridnings- och depositionsberäkningar för en sopförbränningsanläggning i Skövde.

5 Laurin, S. (1986)
Bilavgaser vid intagsplan - Eskilstuna.

6 Robertson, L. (1986)
Koncentrations- och depositionsberäkningar för en sopförbränningsanläggning vid Ryaverken i Borås.

7 Laurin, S. (1986)
Luften i Avesta - föroreningsbidrag från trafiken.

8 Robertson, L., Ring, S. (1986)
Spridningsberäkningar för bromcyan.

9 Wern, L. (1986)
Extrema byvindar i Orrefors.

10 Robertson, L. (1986)
Koncentrations- och depositionsberäkningar för Halmstads avfallsförbränningsanläggning vid Kristinehed.

11 Törnevik, H., Ugnell (1986)
Belastningsprognoser.

12 Joelsson, R. (1986)
Något om användningen av numeriska prognoser på SMHI (i princip rapporten till ECMWF).

13 Krieg, R., Andersson, C. (1986)
Vindmätningar i höga master, kvartalsrapport 4/1985.

14 Dahlgren, L. (1986)
Solmätning vid SMHI.

15 Wern, L. (1986)
Spridningsberäkningar för ett kraftvärmeverk i Sundbyberg.

16 Kindell, S. (1986)
Spridningsberäkningar för Uddevallas fjärrvärmecentral i Hovhult.

17 Häggkvist, K., Persson, Ch., Robertson, L (1986)
Spridningsberäkningar rörande gasutsläpp från ett antal källor inom SSAB Luleåverken.

18 Krieg, R., Wern, L. (1986)
En klimatstudie för Arlanda stad.

19 Vedin, H. (1986)
Extrem arealnederbörd i Sverige.

20 Wern, L. (1986)
Spridningsberäkningar för lösningsmedel i Tibro.

21 Krieg, R., Andersson, C. (1986)
Vindmätningar i höga master - kvartalsrapport 1/1986.

22 Kvick, T. (1986)
Beräkning av vindenergitillgången på några platser i Halland och Bohuslän.

23 Krieg, R., Andersson, C. (1986)
Vindmätningar i höga master - kvartalsrapport 2/1986.

24 Persson, Ch. (SMHI), Rodhe, H. (MISU), De Geer, L.-E. (FOA) (1986) Tjernobylolyckan - En meteorologisk analys av hur radioaktivitet spreds till Sverige.

25 Fredriksson, U. (1986) Spridningsberäkningar för Spendrups bryggeri, Grängesberg.

26 Krieg, R. (1986) Beräkningar av vindenergitillgången på några platser i Skåne.

27 Wern, L., Ring, S. (1986) Spridningsberäkningar, SSAB.

28 Wern, L., Ring, S. (1986) Spridningsberäkningar för ny ugn, SSAB II.

29 Wern, L. (1986) Spridningsberäkningar för Volvo Hallsbergverken.

30 Fredriksson, U. (1986) $SO_2$-halter från Hammarbyverket kring ny arena vid Johanneshov.

31 Persson, Ch., Robertson, L., Häggkvist, K. (1986) Spridningsberäkningar, SSAB - Luleå-verken.

32 Kindell, S., Ring, S. (1986) Spridningsberäkningar för SAABs planerade bilfabrik i Malmö.

33 Wern, L. (1986) Spridningsberäkningar för svavelsyrafabrik i Falun.

34 Wern, L., Ring, S. (1986) Spridningsberäkningar för Västhamns-verket HKV1 i Helsingborg.

35 Persson, Ch., Wern, L. (1986) Beräkningar av svaveldepositionen i Stockholmsområdet.

36 Joelsson, R. (1986) USAs månadsprognoser.

37 Vakant nr.

38 Krieg, R., Andersson, C. (1986) Utemiljön vid Kvarnberget, Lysekil.

39 Häggkvist, K. (1986) Spridningsberäkningar av freon 22 från Ropstens värmepumpverk.

40 Fredriksson, U. (1986) Vindklassificering av en plats på Hemsön.

41 Nilsson, S. (1986) Utvärdering av sommarens (1986) använda konvektionsprognoshjälpmedel.

42 Krieg, R., Kvick, T. (1986) Vindmätningar i höga master.

43 Krieg, R., Fredriksson, U. (1986) Vindarna över Sverige.

44 Robertson, L. (1986) Spridningsberäkningar rörande gasutsläpp vid ScanDust i Landskrona - bestämning av cyanvätehalter.

45 Kvick, T., Krieg, R., Robertson, L. (1986) Vindförhållandena i Sveriges kust- och havsband, rapport nr 2.

46 Fredriksson, U. (1986) Spridningsberäkningar för en planerad panncentral vid Lindsdal utanför Kalmar.

47 Fredriksson, U. (1986) Spridningsberäkningar för Volvo BMs fabrik i Landskrona.

48 Fredriksson, U. (1986) Spridningsberäkningar för ELMO-CALFs fabrik i Svenljunga.

49 Häggkvist, K. (1986) Spridningsberäkningar rörande gasutsläpp från syrgas- och bensenupplag inom SSAB Luleåverken.

50 Wern, L., Fredriksson, U., Ring, S. (1986)
Spridningsberäkningar för lösningsmedel i Tidaholm.

51 Wern, L. (1986)
Spridningsberäkningar för Volvo BM ABs anläggning i Braås.

52 Ericson, K. (1986)
Meteorological measurements performed May 15, 1984, to June, 1984, by the SMHI

53 Wern, L., Fredriksson, U. (1986)
Spridningsberäkning för Kockums Plåt-teknik, Ronneby.

54 Eriksson, B. (1986)
Frekvensanalys av timvisa temperatur-observationer.

55 Wern, L., Kindell, S. (1986)
Luktberäkningar för AB ELMO i Flen.

56 Robertson, L. (1986)
Spridningsberäkningar rörande utsläpp av $NO_x$ inom Fagersta kommun.

57 Kindell, S. (1987)
Luften i Nässjö.

58 Persson, Ch., Robertson, L. (1987)
Spridningsberäkningar rörande gasutsläpp vid ScanDust i Landskrona - bestämning av cyanväte.

59 Bringfelt, B. (1987)
Receptorbaserad partikelmodell för gatumiljömodell för en gata i Nyköping.

60 Robertson, L. (1987)
Spridningsberäkningar för Varbergs kommun. Bestämning av halter av $SO_2$, CO, $NO_x$ samt några kolväten.

61 Vedin, H., Andersson, C. (1987)
E 66 - Linderödsåsen - klimatförhållanden.

62 Wern, L., Fredriksson, U. (1987)
Spridningsberäkningar för Kockums Plåtteknik, Ronneby. 2.

63 Taesler, R., Andersson, C., Wallentin, C., Krieg, R. (1987)
Klimatkorrigering för energiförbrukningen i ett eluppvärmt villaområde.

64 Fredriksson, U. (1987)
Spridningsberäkningar för AB Åetå-Trycks planerade anläggning vid Kungens Kurva.

65 Melgarejo, J. (1987)
Mesoskalig modellering vid SMHI.

66 Häggkvist, K. (1987)
Vindlaster på kordahus vid Alviks Strand - numeriska beräkningar.

67 Persson, Ch. (1987)
Beräkning av lukt och föroreningshalter i luft runt Neste Polyester i Nol.

68 Fredriksson, U., Krieg, R. (1987)
En överskalig klimatstudie för Tornby, Linköping.

69 Häggkvist, K. (1987)
En numerisk modell för beräkning av vertikal momentumtransport i områden med stora råhetselement. Tillämpning på ett energiskogsområde.

70 Lindström, Kjell (1987)
Weather and flying briefing aspects.

71 Häggkvist, K. (1987)
En numerisk modell för beräkning av vertikal momentumtransport i områden med stora råhetselement. En koefficient-bestämning.

72 Liljas, E. (1988)
Förbättrad väderinformation i jordbruket - behov och möjligheter (PROFARM).

73 Andersson, Tage (1988)
Isbildning på flygplan.

74 Andersson, Tage (1988)
Aeronautic wind shear and turbulence. A review for forecasts.

75 Kållberg, P. (1988)
Parameterisering av diabatiska processer i numeriska prognosmodeller.

76 Vedin, H., Eriksson, B. (1988)
Extrem arealnederbörd i Sverige 1881 - 1988.

77 Eriksson, B., Carlsson, B., Dahlström, B. (1989)
Preliminär handledning för korrektion av nederbördsmängder.

78 Liljas, E. (1989)
Torv-väder. Behovsanalys med avseende på väderprognoser och produktion av bränsletorv.

79 Hagmarker, A. (1991)
Satellitmeteorologi.

80 Lövblad, G., Persson, Ch. (1991)
Background report on air pollution situation in the Baltic States - a prefeasibility study.
IVL Publikation B 1038.

81 Alexandersson, H., Karlström, C., Larsson-McCann, S. (1991)
Temperaturen och nederbörden i Sverige 1961-90. Referensnormaler.

82 Vedin, H., Alexandersson, H., Persson, M. (1991)
Utnyttjande av persistens i temperatur och nederbörd för vårflödesprognoser.

83 Moberg, A. (1992)
Lufttemperaturen i Stockholm 1756 - 1990. Historik, inhomogeniteter och urbaniseringseffekt.
Naturgeografiska Institutionen, Stockholms Universitet.

84 Josefsson, W. (1993)
Normalvärden för perioden 1961-90 av globalstrålning och solskenstid i Sverige.

85 Laurin, S., Alexandersson, H. (1994)
Några huvuddrag i det svenska temperatur-klimatet 1961 - 1990.

86 Fredriksson, U. och Ståhl, S. (1994)
En jämförelse mellan automatiska och manuella fältmätningar av temperatur och nederbörd.

87 Alexandersson, H., Eggertsson Karlström, C. och Laurin S. (1997).
Några huvuddrag i det svenska nederbördsklimatet 1961-1990.

88 Mattsson, J., Rummukainen, M. (1998)
Växthuseffekten och klimatet i Norden - en översikt.

89 Kindbom, K., Sjöberg, K., Munthe, J., Peterson, K. (IVL)
Persson, C. Roos, E., Bergström, R. (SMHI). (1998)
Nationell miljöövervakning av luft- och nederbördskemi 1996.

90 Foltescu, V.L., Häggmark, L (1998)
Jämförelse mellan observationer och fält med griddad klimatologisk information.

91 Hultgren, P., Dybbroe, A., Karlsson, K.-G. (1999)
SCANDIA – its accuracy in classifying LOW CLOUDS

92 Hyvarinen, O., Karlsson, K.-G., Dybbroe, A. (1999)
Investigations of NOAA AVHRR/3 1.6 μm imagery for snow, cloud and sunglint discrimination (Nowcasting SAF)

93 Bennartz, R., Thoss, A., Dybbroe, A. and Michelson, D. B. (1999)
Precipitation Analysis from AMSU (Nowcasting SAF)

94 Appelqvist, Peter och Anders Karlsson (1999)
Nationell emissionsdatabas för utsläpp till luft - Förstudie.

95 Persson, Ch., Robertson L. (SMHI)
Thaning, L (LFOA). (2000)
Model for Simulation of Air and Ground Contamination Associated with Nuclear Weapons. An Emergency Preparedness Model.

96 Kindbom K., Svensson A., Sjöberg K., (IVL) Persson C., (SMHI) (2001)
Nationell miljöövervakning av luft- och nederbördskemi 1997, 1998 och 1999.

97 Diamandi, A., Dybbroe, A. (2001)
Nowcasting SAF
Validation of AVHRR cloud products.

98 Foltescu V. L., Persson Ch. (2001)
Beräkningar av moln- och dimdeposition i Sverigemodellen - Resultat för 1997 och 1998.

99 Alexandersson, H. och Eggertsson Karlström, C (2001)
Temperaturen och nederbörden i Sverige 1961-1990. Referensnormaler - utgåva 2.

100 Korpela, A., Dybbroe, A., Thoss, A. (2001)
Nowcasting SAF - Retrieving Cloud Top Temperature and Height in Semi-transparent and Fractional Cloudiness using AVHRR.

101 Josefsson, W. (1989)
Computed global radiation using interpolated, gridded cloudiness from the MESA-BETA analysis compared to measured global radiation.

102 Foltescu, V., Gidhagen, L., Omstedt, G. (2001)
Nomogram för uppskattning av halter av $PM_{10}$ och $NO_2$

103 Omstedt, G., Gidhagen, L., Langner, J. (2002)
Spridning av förbränningsemissioner från småskalig biobränsleeldning
– analys av PM2.5 data från Lycksele med hjälp av två Gaussiska spridningsmodeller.

104 Alexandersson, H. (2002)
Temperatur och nederbörd i Sverige 1860 - 2001

105 Persson, Ch. (2002)
Kvaliteten hos nederbördskemiska mätdata som utnyttjas för dataassimilation i MATCH-Sverige modellen".

106 Mattsson, J., Karlsson, K-G. (2002)
CM-SAF cloud products feasibility study in the inner Arctic region
Part I: Cloud mask studies during the 2001 Oden Arctic expedition

107 Kärner, O., Karlsson, K-G. (2003)
Climate Monitoring SAF - Cloud products feasibility study in the inner Arctic region.
Part II: Evaluation of the variability in radiation and cloud data

108 Persson, Ch., Magnusson, M. (2003)
Kvaliteten i uppmätta nederbördsmängder inom svenska nederbörskemiska stationsnät

109 Omstedt, G., Persson Ch., Skagerström, M (2003)
Vedeldning i småhusområden

110 Alexandersson, H., Vedin, H. (2003)
Dimensionerande regn för mycket små avrinningsområden

111 Alexandersson, H. (2003)
Korrektion av nederbörd enligt enkel klimatologisk metodik

112 Joro, S., Dybbroe, A.(2004)
Nowcasting SAF – IOP
Validating the AVHRR Cloud Top Temperature and Height product using weather radar data
Visiting Scientist report

113 Persson, Ch., Ressner, E., Klein, T. (2004)
Nationell miljöövervakning – MATCH-Sverige modellen
Metod- och resultatsammanställning för åren 1999-2002 samt diskussion av osäkerheter, trender och miljömål

114 Josefsson, W. (2004)
UV-radiation measured in Norrköping 1983-2003.

115 Martin, Judit, (2004)
Var tredje timme – Livet som väderobservatör

116 Gidhagen, L., Johansson, C., Törnquist, L. (2004)NORDIC – A database for

evaluation of dispersion models on the local, urban and regional scale

117 Langner, J., Bergström, R., Klein, T., Skagerström, M. (2004)
Nuläge och scenarier för inverkan på marknära ozon av emissioner från Västra Götalands län – Beräkningar för 1999

118 Trolez, M., Tetzlaff, A., Karlsson, K-G. (2005)
CM-SAF Validating the Cloud Top Height product using LIDAR data

119 Rummukainen, M. (2005)
Växthuseffekten

120 Omstedt, G. (2006)
Utvärdering av $PM_{10}$ - mätningar i några olika nordiska trafikmiljöer

121 Alexandersson, H. (2006)
Vindstatistik för Sverige 1961-2004

122 Samuelsson, P., Gollvik, S., Ullerstig, A., (2006)
The land-surface scheme of the Rossby Centre regional atmospheric climate model (RCA3)

123 Omstedt, G. (2007)
VEDAIR – ett internetverktyg för beräkning av luftkvalitet vid småskalig biobränsleeldning
*Modellbeskrivning och slutrapport mars 2007*

124 Persson, G., Strandberg, G., Bärring, L., Kjellström, E. (2007)
Beräknade temperaturförhållanden för tre platser i Sverige – perioderna 1961-1990 och 2011-2040

125 Engardt, M., Foltescu, V. (2007)
Luftföroreningar i Europa under framtida klimat

126 Jansson, A., Josefsson, W. (2007)
Modelling of surface global radiation and CIE-weighted UV-radiation for the period 1980-2000

127 Johnston, S., Karlsson, K-G. (2007)
METEOSAT 8 SEVIRI and NOAA Cloud Products. A Climate Monitoring SAF Comparison Study

128 Eliasson, S., Tetzlaf, A., Karlsson, K-G. (2007)
Prototyping an improved PPS cloud detection for the Arctic polar night

129 Trolez, M., Karlsson, K-G., Johnston, S., Albert, P (2008)
The impact of varying NWP background information on CM-SAF cloud products

130 Josefsson, W., Ottosson Löfvenius, M (2008)
Total ozone from zenith radiance measurements. An empirical model approach

131 Willén, U (2008)
Preliminary use of CM-SAF cloud and radiation products for evaluation of regional climate simulations

132 Bergström, R (2008)
TESS Traffic Emissions, Socioeconomic valuation and Socioeconomic measures Part 2:
Exposure of the European population to atmospheric particles (PM) caused by emissions in Stockholm

133 Andersson, S., Bergström, R., Omstedt, G., Engardt, M (2008)
Dagens och framtidens partikelhalter i Sverige. Utredning av exponerings-minskningsmål för PM2.5 enligt nytt luftdirektiv

134 Omstedt, G., Andersson, S (2008)
Vintervägar med eller utan dubbdäck. Beräkningar av emissioner och halter av partiklar för olika dubbdäcksscenarier

135 Omstedt, G., Andersson, S., Johansson, Ch., Löfgren, B-E (2008)
Luftkvalitet och småskalig biobränsle-eldning. Tillämpningar av SIMAIRved för några kommuner

136 Josefsson, W., Ottosson Löfvenius, M (2009)
Measurements of total ozone 2006-2008

137 Andersson, S., Omstedt, G (2009)
Validering av SIMAIR mot mätningar av PM10, $NO_2$ och bensen.
Utvärdering för svenska tätorter och trafikmiljöer avseende är 2004 och 2005

138 Wern, L., Bärring, L (2009)
Sveriges vindklimat 1901 – 2008
Analys av förändring i geostrofisk vind

139 Wern, L., German, J (2009)
Korttidsnederbörd i Sverige, 1995 – 2008

140 Omstedt, G., Andersson, S., Bergström., R (2010)
Dagens och framtidens luftkvalitet i Sverige. Haltberäkningar av $NO_2$, PM10 och PM2.5 i svenska trafikmiljöer för framtidsscenarier med minskade europeiska emissioner

141 Wern, L., Isaksson, L (2010)
Åska i Sverige 2002 – 2009

142 Andersson, S., Omstedt, G., Robertson, L (2010)
Känslighetsanalys, vidareutveckling och validering av SIMAIRs urbana spridnings-modell BUM

143 Wern L., (2012)
Extrem nederbörd i Sverige
under 1 till 30 dygn, 1900 – 2011

144 Omstedt, G., Andersson, S., Bennet, C., Bergström, R., Gidhagen, L., Johansson, Ch., Persson, K (2010)
Kartläggning av partiklar i Sverige – halter, källbidrag och kunskapsluckor

145 Engardt, M., Andersson, C., Bergström, R (2010)
Modellering av Marknära Ozon
- Regionala och högupplösta tillämpningar av MATCH

146 Omstedt, G., Forsberg, B., Nerhagen, L., Gidhagen, L., Andersson, S (2011)
**SIMAIR**scenario – ett modellverktyg för bedömning av luftföroreningars hälsoeffekter och kostnader

147 Andersson, C., Andersson, S., Langner, J och Segersson, D (2011)
Halter och deposition av luftföroreningar - Förändring över Sverige från 2010 till 2020 i bidrag från Sverige, Europa och Internationell Sjöfart

148 Carlund, Th (2011)
Upgrade of SMHI's meteorological radiation network 2006-2007 – Effects on direct and global solar radiation

149 Josefsson, W., Ottosson Löfvenius, M (2012)
Measurements of total ozone 2009-2011

150 Omstedt, G., Andersson, S., Asker, Ch., Jones, J., Kindell, S., Segersson, D., Torstensson, M (2012)
Luftkvaliten i Sverige år 2020
Uppföljning av miljömålet Frisk luft för trafikmiljöer i svenska tätorter

151 Omstedt, G., Burman, L. SLB-analys, (2012)
Beräkningar av kväveoxidhalter vid några gator i Umeå åren 2014 och 2020 med och utan miljözon

152 Stefan Andersson och Gunnar Omstedt (2013)
Utvärdering av SIMAIR mot mätningar av PM10 och NO2 i Göteborg, Stockholm och Umeå för åren 2006-2009.
Undersökning av en ny emissionsmodell för vägtrafikens slitagepartiklar.

153. Segersson, David (2014)
A dynamic model for shipping emissions - Adaptation of Airviro and application in the Baltic Sea

154. Wern, Lennart. (2013)
Luftfuktighet, Variationer i Sverige

155. Holmin-Fridell, Sofi. Jörgen Jones, Cecilia Bennet, Helena Södergren, Sven Kindell, Stefan Andersson, Martin Torstensson och Mattias Jakobsson. (2013) Luftkvaliteten i Sverige år 2030.

156. Gunnar Omstedt, Bertil Forsberg*, Karin Persson**, *Umeå Universitet, **IVL Svenska Miljöinstitutet (2014) Vedrök i Västerbotten - mätningar, beräkningar och hälsokonsekvenser.

ISSN 0283-7722

Sveriges meteorologiska och hydrologiska institut
601 76 Norrköping
Tel 011-495 80 00  Fax 011-495 80 01